MANUFACTURABILITY AND BENDING PERFORMANCE OF GRADED STEEL STRUCTURES FABRICATED BY SELECTIVE LASER MELTING

A Thesis

by

OMPRAKASH DAS

Submitted to the Office of Graduate and Professional Studies of
Texas A&M University
in partial fulfillment of the requirements for the degree of

MASTER OF SCIENCE

Chair of Committee,   ChaBum Lee
Co-Chair of Committee, Mathew A. Kuttolamadom
Committee Members,   Jyhwen Wang

Head of Department,   Andreas Polucarpou

May 2021

Major Subject: Mechanical Engineering

ABSTRACT

The objective of this research work is to investigate the processing, structure, properties, and performance of stiffness/hardness-graded stainless steel 316L bulk samples fabricated via selective laser melting (SLM) additive manufacturing. By systematically altering the location-specific volumetric energy density imparted (via process-parameter change), variations in microstructure and density can be achieved; these result in intended changes to mechanical properties such as moduli, hardness, etc. Based on a design of experiments, ASTM-standard samples that have mechanical property gradations as a function of the distance from the neutral axis were fabricated to evaluate performance when subjected to standard bending tests. Digital image correlation (DIC) was employed to capture local and global deformation. Further, the characteristics of each of the zones, as well as interfaces between zones were investigated via microscopy and indentation testing. Altogether, this study is expected to provide insights into the additive manufacturability of such spatially tailored structures, their resulting property distributions, and their performance in various engineering applications.

ACKNOWLEDGEMENTS

I would like to thank my committee chair, Dr. Lee, my committee co-chair, Dr. Kuttolamadom, and my committee member, Dr. Wang for their guidance and support throughout the course of this research. I would also like to thank the head of the department, Dr. Rasmussen, for all his support during my time in this program.

Thanks also go to my friends and colleagues and the department faculty and staff for making my time at Texas A&M University a great experience.

Finally, thanks to my family for their encouragement throughout this process.

CONTRIBUTORS AND FUNDING SOURCES

NOMENCLATURE

FGM	Functionally graded material
SLM	Selective laser melting
AM	Additive manufacturing
DIC	Digital image correlation
SS	Stainless steel
DOE	Design of experiments

TABLE OF CONTENTS

LIST OF FIGURES

LIST OF TABLES

INTRODUCTION

Materials having gradient porosity, composition, and/or microstructure within their volume are called functionally graded materials (FGMs). This variation throughout the volume of the material results in varying mechanical and thermal properties that are dependent on the spatial position of the material. The gradation can be continuous or stepwise that is depending on the fabricator and their intended use.

The manufacturing and fabrication of FGMs can be done by conventional manufacturing processes as well as additive manufacturing techniques. Depending on the type of FGMs required and their application field the manufacturing process is selected. The conventional methods include powder metallurgy, Centrifugal casting, and Tape casting process. The additive manufacturing methods include Material Extrusion, Powder-Bed Fusion, Directed-Energy Deposition, and Sheet Lamination. By implementing powder bed fusion single material FGMs can be fabricated by controlling various process parameters like laser power, exposure time, etc. this will result in produce structures having gradient microstructures throughout its volume hence it will have variation in micro elastic modulus as well as other mechanical properties like hardness, toughness, etc. These kinds of structures possess certain performance-related advantages like lower stresses, lower strains, higher wear resistance, fatigue resistance, etc.

Functionally grading a non-lattice-based single metallic alloy can be achieved using additive manufacturing. Selective laser sintering and selective laser melting processes can be employed to create functionally graded samples that are composed of a single metallic alloy like SS316. By varying laser power and laser exposure time for different layers during fabrication a stepwise or continuous gradient

structure can be fabricated. these parameters various will result in the intended mechanical property like elastic modulus, hardness, etc. variation throughout the volume of the structure.

For a given bending scenario we can limit peak normal stress or normal strain to a lower value compared to a homogenous sample. After preliminary analytical analysis, we believe that when subjected to bending load, depending on the arrangement of the graded zones a lower maximum normal stress or maximum normal strain is achievable compared to a homogeneous sample having equivalent flexural rigidity. we can achieve a lower or higher total transverse deflection compared to a homogenous structure depending on the configuration of gradation layers: Under the bending scenario, we think that the total transverse deformation can be altered desirable to a certain application by configuring and aligning the graded zones accordingly. Consequently, we can achieve equivalent allowable stress, strain, and transverse deflection under a certain bending load using less material (lower mass and volume). to achieve certain peak stress or strain we will be using less material as the sample size required to achieve those values will be smaller in dimension.

BACKGROUND AND LITERATURE REVIEW

2.1. Background

2.1.1. Types of FGMs

Generally, FGMs are classified into three categories porosity gradient structured FGM, chemical composition gradient-structured FGMs, and microstructural gradient-structured FGMs. Microstructure Gradient FGMs: In such FGMs the microstructure within a material is varied in a continuous or stepwise pattern to achieve a desired mechanical or thermal property. The gradation in microstructure is most often achieved during the solidification process by controlling the rate of solidification throughout the volume of the material. Controlled heat treatment can also be implemented to achieve such graded FGMs. The gradation would lead to a gradual change of the material properties with respect to the spatial positions of the material since properties are directly related to the microstructure. The microstructural gradient FGMs are generally used in components having a very hard surface that would resist wear and would have a tough core that would resist high impacts that takes place while in operation.

Chemical composition gradient structure FGMs: In such FGMs the chemical composition throughout the thickness is altered in a continuous or stepwise manner relative to the spatial position within the volume of the material. The alteration could be in the form of either single-phase or multiphase material. Usually, powder metallurgy is used to manufacture such types of functionally graded materials where the powder is used in a layer-by-layer pattern and then compacted using a sintering or hot-pressing process.

Porosity gradient structure FGMs: In such FGMs the porosity is altered throughout the material in a continuous or stepwise manner. The size or density of the pores varies depending on the field of application to achieve the required property. Generally, such functionally graded materials are used in biomedical fields mostly for creating implants like bones, teeth, etc. The human body consists of many structures with varying porosity, as a result, these type of FGM implants helps in easier integration in the body compared to a conventional implant.

2.1.2. Application of Functionally Graded Materials:

FGMs have been used in a lot of applications in many domains that include automobiles, defense, aerospace, biomedical, electrical, electronics, energy, optoelectronics, marines, thermo-electronics, and many others. FGMs are greatly utilized in applications having extreme working conditions like having wear-resistant linings to handle abrasive ore particles in the mining industry, for providing resistance to crack initiation, heat shields for the rocket, for the heat engine components, for heat exchanger tubes, for the plasma facings for fusion reactors in nuclear reactor plant, for thermo-electric generators, and in the electrical insulating applications.

In the future, requirements for FGMs will be in such applications, where extreme mechanical, thermal, and chemical properties/performance are required, that will be able to sustain such severe operating conditions. The application areas for functionally graded materials will expand in the future when the cost of production for manufacturing/engineering such novel materials are trimmed down. The use of functionally graded materials is now seen as one of the most important, effective, and efficient materials for promoting sustainable development in industries.

2.2. Literature Review

2.2.1. Manufacturability of FGMs

For manufacturing FGMs both conventional manufacturing processes, as well as additive manufacturing methods, can be applied. Usually, the manufacturing process selection for FGMs depends upon the kind of FGMs required and their applicability. Centrifugal casting, powder metallurgy, and Tape casting are some of the most used conventional manufacturing methods for manufacturing FGMs. The additive manufacturing processes for fabricating FGMs include processes like Directed-Energy Deposition, Material Extrusion, Sheet Lamination, Powder-Bed Fusion, etc.

2.2.1.1. Conventional manufacturing of FGMs:

2.2.1.1.1 Powder Metallurgy:

The steps for fabricating FGMs using this technique involve prepare the powder materials, then process the powder, then forming operations, and then sintering or pressure-assisted hot consolidation— depends on the service requirement of the FGMs that is getting manufactured. After that variation in composition is achieved in the green part by stacking the graded powder. After the production of the graded green part, the green part is consolidated through hot pressing or sintering.

A wide range of control of microstructure and composition can be achieved having near-net-shape forming capability using powder metallurgy. A lot of different types of materials can be fabricated through this method. Powder metallurgy is very efficient in terms of energy, time as well as cost of production.it is very easy to operate and extremely good for mass production. The main drawbacks of the powder metallurgy process are the inability to manufacture highly intricate parts, limited control over all the processing parameters to achieve proper gradation, and limited strength of the final part.

A metal-metal (Al-Cu) FGM was manufactured using Powder metallurgy [1], they used aluminum powder and copper powder with varying weight % of each component.

5

2.2.1.1.2. The Centrifugal Casting Method

In the centrifugal casting method, molten material that containing another reinforcing material—either in solid or in the molten state— is poured into a mold. The mold is inside a rotating die. The rotation of the die generates a centrifugal force. This centrifugal force draws the molten material towards the mold and creates a partition between the two types of material—it also melts the two materials. This happens because of the density difference between the two materials, resulting in the production of a functionally graded material. The gradation of the FGM produced by the centrifugal casting process is significantly influenced by the processing parameters, like density difference among the molten material and the reinforcing powder material, molten material's viscosity, the size of the particle, and the particle size distribution in the powder, the, and the time required for the solidification.

The major advantage of utilizing the centrifugal casting method to fabricate FGMs is that continuous gradation is achievable relatively easily using this process. The limitations of the centrifugal casting to manufacture FGMs are the following: Only cylindrical sections like the bushing, tube, and tubular or cylindrical castings can be produced that are very simple in shape. The gradation is limited by the density difference between the constituent materials, and the centrifugal force.

2.2.1.1.2. The Tape Casting Method:

In the tape casting process, a slurry mixture is created that contains a mixture of different materials that are put into an organic solvent having suitable plasticizers and binders. The slurry mixture is spread onto a moving belt, and then the moving belt is passed under a blade edge that converts the slurry into a constant thickness tape. Then the solvent gets dried off, resulting in the formation of the

green part. Stepwise gradation of functionally graded materials is produced by stacking those tapes of different compositions. Then sintering is done on the stack of tapes under a pressure of about 3–30 MPa and a temperature from 50° to 200 °C.

The advantage of this process is that high-resolution functionally graded materials can be produced using this method. The disadvantage of this process is the limited strength of the final product that is very dependent on the pressure and temperature of the sintering process.

2.2.1.2. Additive manufacturing of FGMs

Recent advancements in AM processes have created many possibilities to fabricate fully dense metallic parts. At present time, customized parts can be procured in a very short time using digital data. One of the major areas of interest in these processes is the possibility to manufacture parts made as functionally graded materials (FGM). For now, this field is limited to studies on the manufacturability of discrete functionally graded materials that consist of homogeneous material layers with a small modification of material after several layers or nearly continuous FGM on samples.

Several AM technologies have been classified into seven broad classes by the ASTM F42 technical committee. These classes are Vat Photopolymerization, Material Jetting, Binder Jetting, Material Extrusion, Powder-Bed Fusion, Sheet Lamination, and Directed-Energy Deposition. four out of these seven classes are currently being utilized to produce FGM parts. Those are Material Extrusion; Directed-Energy Deposition; Powder-Bed Fusion; and sheet lamination.

AM technology uses 5 basic steps to reach the final product fabrication:

1. Generating the computer-aided design (CAD) file of the FGM part.

2. Converting the CAD file into a standard triangulation language (STL) file or additive manufacturing file (AMF)

3. Receiving the STL/AMF file into the AM machine and slicing that file into two-dimensional layers of triangles that represent the 3D CAD data.

4. Building up the part layer by layer that follows the path governed by 2D sliced CAD data.

5. Removing the part from the machine and performing residual operations like heat treatment and support structure removal.

2.2.1.2.1. Material Extrusion:

Fused-deposition modeling (FDM) falls in this class of AM processes. A wire-like filament material is used to create the three-dimensional FGM part, layer-by-layer. The filament is heated and extruded through a nozzle at a certain rate that gets deposited layer-after layer. This method is utilized to produce, functional parts, parts made with FGMs, and prototypes.

A process called Freeze-form Extrusion Fabrication (FEF) is also classified in material-extrusion AM processes. Computer-controlled extrusion and deposition are used to produce a 3D FGM part layer-after layer in this technology. The FEF is also used for manufacturing FGMs.

2.2.1.2.2. Powder-Bed Fusion:

The powder-bed fusion (PBF) process is a type of AM in which building platform is used as a bed onto which the powdered material is spread over, the powder is then scanned by a laser beam, or an electron beam, along the path determined by the 2D CAD profile that has been sliced from the 3D CAD file. The process takes place layer by layer so once a layer gets scanned, the building platform gets lowered by a certain layer thickness distance. A fresh batch of powder is then spread over the scanned layer and the scanning process is repeated for the entire manufacturing completion.

The selective laser melting (SLM), the selective-laser sintering (SLS), the selective-heat sintering (SHS), and the electron-beam melting (EBM) are the AM processes that belong in the powder bed fusion class of additive manufacturing. A laser, or an electron beam, is used as a power source that

fuses or melts the powdered material in PBF processes. The major difference between the SLM and the SLS process is that the laser melts the powder in the SLM process whereas it fuses the powder in the SLS process. The SHS process is different from other PBF processes; in that, a heated thermal print head is used to fuse the powder instead of a laser. A vacuum is required for creating FGM parts using the EBM process.

In the SLS process, the building's platform chamber's temperature is controlled; and is usually kept a bit below the melting temperature of the material. The powder material used in the SLS process is recyclable and reusable hence the material efficiency is very high for this AM process. Generally, the final produced parts using SLS are porous; as a result, those parts are most suitable to produce parts or FGM parts with the necessary porosity or porosity gradation, like biomedical implants, and parts made up of FGM. To produce very dense parts SLM process is used. The advantages of using SLM are that process is faster than SLS and produces higher strength and denser parts. The selective laser melting process has few disadvantages like the process is very energy-intensive resulting in poor energy efficiency of about 10–20%. The SLM process is can be used to manufacture FGMs.

The selective heat sintering process requires the use of a heated-print head that fuses the powder. A roller is used to spread the layers of powder; the heated-print head is passed through as a power source that fuses the powder in the path determined by the 2D CAD file sliced data. Then the platform gets lowered by one-layer thickness, and the new layer of powder is spread over the already printed layer, and the whole process is repeated until the part gets fabricated.

The electron beam melting (EBM) process is very similar to SLM and the SLS processes. The most notable difference is the power source, the electron beam is used as the power source instead of a laser. EMB is used to produce only metal parts compared to SLM and SLS processes that can manufacture metals, composite materials, as well as ceramics. The major advantages of EBM are that it

is very fast (nearly 5-10 times faster than other AM methods) and a very energy-efficient process with up to 95% efficiency.

2.2.1.2.3. Directed-Energy Deposition

Directed-Energy Deposition (DED) is a type of AM process that uses energy source like electron beam, plasma, or laser to produce a melt pool on the substrate, and the wire or powder material that is aligned coaxially for the source of energy is delivered into that melt pool on the substrate. The process results in creating a solid material track upon the completion of the solidification of the melt pool. Layer by layer this process is repeated to manufacture the 3D part. the electron-beam deposition and the laser-metal deposition process (LMD) processes fall into this category of AM technology. These processes have also been used to fabricate FGM parts.

2.2.1.3. Additive manufacturability of SS316L and graded stainless steel structures:

2.2.1.3.1. Functionally Graded Additively Manufactured materials (FGAMs)

A radical change to performance modeling from contour modeling by incorporating performance-driven functionality directly into the material is established by Functionally Graded Additive Manufacturing (FGAM). We can strategically control the density, microstructure, porosity of the composition or can mix distinct materials to build a seamless monolithic structure using FGAM. An in-depth fundamental conceptual understanding of FGAM processes including present technologies that can be implemented to fabricate FGAM parts has been provided in this research work[2]. They have presented all the advantages as well as limitations of various FGAM processes in detail. Directed energy deposition method was used in this research work to manufacture functionally graded material from Ti-6Al-4V to Invar 36 (64 wt% Fe, 36 wt% Ni), they investigated the microstructure, phases, composition, and microhardness of those materials[3]. Freeze-form Extrusion Fabrication (FEF) has been

10

implemented to manufacture functionally graded 3D materials in this work[4]. They have demonstrated

the efficiency and effectiveness of the FEF system by producing limestone ($CaCO_3$) and then producing

compositionally graded green parts of alumina (Al_2O_3) and zirconia (ZrO_2). The fabricated parts were

analyzed to determine the material composition using energy dispersive spectroscopy (EDS). Most of

the multi-material parts fabricated using additive manufacturing processes are not necessarily functional.

To achieve functional and complex parts from additive manufacturing a proper process and processing

parameter control must be established. this research work deals with the approach to achieve such global

control to get functionally graded parts using additive manufacturing (direct laser deposition)[5]. The

applicability of Electron Beam Melting (EBM) has been researched in manufacturing FGM parts in this

research work[6]. They developed a multi-scale heat transfer model and investigated the

manufacturability of FGM parts by the EBM process.

2.2.1.3.2. Laser-based FGAMs

laser deposition system has been employed in this research work to manufacture and develop a

process and parameter control to manufacture FGM parts[5]. It facilitated in selecting an adaptive way

of manufacturing strategy to control parameters to get desired distribution of material and geometry. For

fabricating functionally graded materials a novel hybrid AM technology has been proposed in this

research work[7]. They have coupled selective laser melting (SLM) and cold spraying (CS) to fabricate

Al-Ti6Al4V compositionally graded samples. FGM parts made from titanium alloy composites have

been fabricated using Laser metal deposition (LMD) technology in this research paper[8]. They

optimized the various processing parameters to obtain graded material compositions and then

tribological, metallurgical, and mechanical studies on those samples have been done. Their conclusion

showed that FGM parts generated using this technique by varying the processing parameters exhibited

improved property compared to parts made by keeping parameters constant. In this research work, the authors have provided an in depth progress overview on the fabrication of FGM metallic parts using laser metal deposition (LMD)[9]. They have also identified all the advantages of fabricating metallic FGMs using this method as well as challenges associated with it.

2.2.1.3.3. 316L/ steel FGMs

Functionally graded materials of two different patterns fabricated by gradually changing the percentages of steel 316L from 100% to 100% Inconel718 superalloy by implementing laser engineered net shaping AM process in this research work[10]. They have also characterized composition, microstructure, and microhardness along the direction of gradation by investigating those FGM parts. The laser-based AM process of directed energy deposition (DED) has been implemented to manufacture metallic FGMs having compositional gradient made from 304L stainless steel and Inconel 625 in this work [11]. Chemistry, phase composition, microstructure, and microhardness as a function of spatial position were investigated and characterized in this study. FGMs made from stainless steel 316 (STS316)/Fe were manufactured by direct energy deposition (DED) technology using laser as a power source in this research paper[12]. Defects and microstructures were investigated by using scanning electron microscope (SEM) technology. Electron Beam Melting (EBM) has been used to manufacture graded SS316L with 99.8% relative density in this work[13]. they have also done a feasibility study of the manufacturability of such parts using this AM technology.

2.2.1.3.4. Laser-based SS316L FGMs

Functionally graded stainless-steel alloys material has been manufactured using selective laser melting (SLM) process in this work[14]. They have varied various process parameters during the

fabrication step to manipulate the microstructure of the final fabricated FGM samples. Laser Metal Deposition Shaping (LMDS) was implemented to fabricate stainless steel (SS) 316 parts in this paper[15]. They have characterized the composition, microstructure, and phase using Scanning Electron Microscope (SEM) and X-ray diffraction (XRD). They have reported some samples having fabrication defects. They have also tested for obtaining mechanical properties. A comparison has been done to understand critical parameters influencing the microstructures and properties. Their results suggest that microstructure of SS 316 is comprised of dendrites growing epitaxially from the substrate. The mechanical properties were anisotropic, but the composition was uniform.

2.2.1.4. Applications of FGMs:

Functionally graded materials are a novel class of materials having unique characteristics. FGMs find applicability in thermal protection of space vehicles, medical implants, thermoelectric converter, etc. since FGMs are very versatile materials that can be used as nano, optoelectronic and thermoelectric materials. In the future, the demand will grow for FGMs that can have extraordinary mechanical, electronic, and thermal properties such that those will be able to sustain harsh environmental conditions and are easily available at a reasonable price.

This paper discusses various possibilities in terms of the application of FGMs in biomedical fields. FGMs are getting utilized more and more in orthopedic prostheses since the functional gradient can be employed to reproduce identical local properties of the actual bone, this assists in reducing shear stress between the implant and the neighboring tissues as well as minimizing the stress shielding effect. The work describes all these in detail [16].

Engine components in modern aero vehicles experiences extremely demanding operating conditions with excessive fatigue cycles, high wear rate, and severe thermal attack. In such conditions

13

properly designed Functionally graded structures can have better flexibility in composition or properties resulting in improved performance in withstanding such demanding conditions. Laser engineering net shaping can be used to fabricate such material.[17] This paper presents a better understanding of processing parameters and their influence on the fabrication of functionally graded stainless steel, which affects the final part quality. [18]In this paper, the different wear failures were discussed in the various modes of transport. They have discussed the application of FGMs as a preventive measure.

2.2.1.5. Bending performance of additively manufactured SS316L/FGM structures:

There is a need to analyze the bending, fracture, and fatigue characteristics of FGM structures in comparison to regular materials. [19]This research work deals with the investigation of FGMs under bending loads as well as under vibration and buckling. FEA has also been employed in this work to validate the bending performance. This study deals with the characterization of functionally graded syntactic foams (FGSFs)'s flexural properties[20]. They have performed flexural testing to make the conclusions and employed analytical and FEA analysis to validate their results. The bending and buckling performance of functionally graded annular microplates have been investigated in this research work[21]. They have assumed the material property to vary along with the thickness and implemented modified couple stress theory and Mindlin plate theory to analyze the performance of FGM annular microplates. Fractography study of functionally graded composite made from 3YPSZ/316L has been done after subjecting those samples to indentation and flexural bending tests in this work[22]. They analyzed the morphological section of layers by optical microscopy and scanning electron microscopy.

2.3. Research Gaps and Motivations

By implementing powder bed fusion single material FGMs can be fabricated by controlling various process parameters like laser power, exposure time, etc. these will result in structures having gradient microstructures throughout their volume hence they will have variation in micro elastic modulus. These kinds of structures possess certain performance-related advantages like lower stresses, lower strains, higher wear resistance, etc.

- Functionally grading a non-lattice-based single metallic alloy can be achieved using additive manufacturing. Selective laser sintering and selective laser melting processes can be employed to create functionally graded samples that are composed of a single metallic alloy like SS316. By varying laser power and laser exposure time for different layers during fabrication a stepwise or continuous gradient structure can be fabricated. these parameters various will result in the intended mechanical property like elastic modulus, hardness, etc. variation throughout the volume of the structure.

- For a given bending scenario we can limit peak normal stress or normal strain to a lower value compared to a homogenous sample. After preliminary analytical analysis, we believe that when subjected to bending load, depending on the arrangement of the graded zones a lower maximum normal stress or maximum normal strain is achievable compared to a homogeneous sample having equivalent flexural rigidity.

- We can achieve a lower or higher total transverse deflection compared to a homogenous structure depending on the configuration of gradation layers: Under the bending scenario, we think that the total transverse deformation can be altered desirable to a certain application by configuring and aligning the graded zones accordingly.

- Consequently, we can achieve equivalent allowable stress, strain, and transverse deflection under a certain bending load using less material (lower mass and volume). to achieve certain peak stress or strain we will be using less material as the sample size required to achieve those values will be smaller in dimension.

- Limited research on the application of laser-based AM to functionally grade a non-lattice-based single metallic alloy like SS316L.

- Leverage AM for creating FGMs by exploiting the flexibility and control over various parameters.

- Tune the mechanical performance of SS316L FGAMs under bending (Stress, strain)

- Applicability to structures with geometric/space constraints (different deflection for the same cross-section)

- Tune the surface properties (wear resistance, inhibition of crack initiation, etc.

From the above literature survey, we can conclude that limited research has been done regarding the application of laser-based AM to functionally grade a non-lattice-based single metallic alloy like SS316L or any other single metallic alloy by creating microstructural or porosity gradient throughout the volume of a part. So, more research work should be done as there is a big possibility that better steel/SS316L/metallic FGMs with very efficient functionality can be produced economically and sustainably using laser-based AMs. From the literature survey, we can also say that there has been a lack of research on the mechanical as well as thermal performance evaluation and characterization of laser-based additively manufactured functionally graded metallic alloys like SS316L. An extensive tensile, bending, fatigue, wear performance evaluation of such FGM structure can lead to a much better

application of metallic alloys like SS316L in various engineering fields. This research intends to investigate such areas.

MATERIALS AND METHODS

3.1. Materials:

Non-lattice-based single metallic alloys like SS316L is a very useful material for most industries. The powder used in the AM machine that will be used in this research work is SS 316L-0407. This stainless-steel alloy is austenitic that comprises iron alloyed with up to 18% (mass fraction) of chromium of mass fraction, up to 14% of nickel, and up to 3% molybdenum, along with other minor elements. Compared to standard 316L alloy this alloy is an extra-low carbon variation. Due to this, this powder alloy is resistant to sensitization (i.e. precipitation of carbide at grain boundaries) and has good characteristics for welding. Apart from that, it has low stress to rupture and tensile strength at high temperatures.

The powder has the following noticeable material properties:

- High hardness
- High toughness
- High machine-ability
- High corrosion resistance
- Can be highly polished

The basic properties and the complete chemical composition of the SS 316L-0407 powder have been provided in table 1 and table 2.

Table 1.SS 316L-0407 specifications and data

Density	7.99 g/cm³
Thermal conductivity	16.2 W/mK
Melting range	1371 °C to 1399 °C
Coefficient of thermal expansion	16 10-6 K-1

Table 2. Composition of SS 316L-0407 powder

Element	Mass (%)
Iron	Balance
Chromium	16.00 to 18.00
Nickel	10.00 to 14.00
Molybdenum	2.00 to 3.00
Manganese	≤ 2.00
Silicon	≤ 1.00
Nitrogen	≤ 0.10
Oxygen	≤ 0.10
Phosphorus	≤ 0.045
Carbon	≤ 0.03
Sulfur	≤ 0.03

Renishaw AM400 metal additive manufacturing system has been used to print/manufacture all the samples. The system offers great flexibility in producing homogeneous as well as FGM samples. Using this machine, we were able to change processing parameters conveniently to achieve desired gradation throughout the samples.

Some process specification employed on Renishaw AM400 on default has been provided in table 3.

Table 3. Process specification (default):

Powder description	Stainless steel powder (SS 316L-0407)
Layer thickness	50 μm
Exposure time	80 μs
Laser power	200 W
Additive manufacturing system	AM400

Using these specifications, the printed parts are expected to have the following mechanical properties given in Table 4.

Table 4. Mechanical properties of default samples (provided by OEM manufacturer)

	As-Built
Upper tensile strength (UTS)[1]	
Horizontal direction (XY)	676 MPa ±2 MPa
Vertical direction (Z)0	624 MPa ±17 MPa
Yield strength[1]	
Horizontal direction (XY)	547 MPa ±3 MPa
Vertical direction (Z)	494 MPa ±14 MPa
Elongation at break[1]	
Horizontal direction (XY)	43% ±2%
Vertical direction (Z)	35% ±8%
Modulus of elasticity[1]	
Horizontal direction (XY)	197 GPa ±4 GPa

Table 4 continued

	As-Built
Vertical direction (Z)	190 GPa ±10 GPa
Hardness (Vickers)2	
Horizontal direction (XY)	198 HV0.5 ±8 HV0.5
Vertical direction (Z)	208 HV0.5 ±6 HV0.5
Surface roughness (Ra)[3]	
Horizontal direction (XY)	4 μm to 6 μm
Vertical direction (Z)	4 µm to 6 µm

[1]Tested at ambient temperature by Nadcap and UKAS accredited independent laboratory. Test

ASTM E8. Machined before testing.

[2]Tested to ASTM E384-11, after polishing.

[3]Tested to JIS B 0601-2001 (ISO 97), after bead blasting

3.2. Methods

3.2.1. Design of Experiments (DOE):

Based on related results, the design of experiments (DOE) was generated to determine the

parameters that would provide an appreciable difference in hardness and elastic modulus. From the DOE

and preliminary experiments, we found the following parameter sets that yielded different hardness

values and nano indented elastic modulus.

Table 5. Design of Experiments (DOE)

No.	Power P [W]	Scanning Speed, v [mm/s]	P/v, [J/m m]	Energy density [J/mm³]	Hardness [HV.5]	Exposure Time T [μs]	E (Elastic modulus) (GPa)
1	200	698	0.29	52.1	318	74	162.99
2	150	800	0.19	34.1	294	63	154.09
3	200	750	0.27	48.5	271	68	187.48
4	200	577	0.35	63.0	256	92	211.03
5	175	800	0.22	39.8	209	63	203.92
6/ Default	200	652	0.31	55.8	261	80	197±4

From DOE the laser power to manufacture the parts will be varied in 3 levels i.e. 150 W, 175 W, and 200W. the exposure time will be varied from 60 µs to 92 µs. the layer thickness will be kept constant at 50µm, point distance will be maintained at 60 µm, and hatch spacing will be kept at 110 µm

3.2.2. Sample design and configurations:

3.2.2.1. Bending samples:

Since our intended was to evaluate bending performance for the functionally graded samples it was advantageous for us to use a four-point bending standard instead of a three-point bending standard because of the following reasons:

- A 3-point bending test is recommended for homogeneous material whereas a 4-point bending test is suited for non-homogeneous material like composites, FGMs, etc. To avoid premature failure.

- 4-Point fixtures produce peak stress along an extended region of the specimen so exposing a larger volume of the specimen with potential defects and flaws to be highlighted.

- The 4-point test produces pure bending over a significant region whereas the bending in 3-point is complicated (bending as well as shear) hence measuring mechanical properties is easier in the 4-point bending test.

Since steel and other metals are non-graded/ homogeneous in volume most of the flexural bending standards used are three-point bending standards, hence I followed ASTM C1161 − 18 Standard (Standard Test Method for Flexural Strength of Advanced Ceramics at Ambient Temperature) for four-point bending.

According to this standard, the dimensions of the samples were selected to be length: 50 mm (span length(L)- 40 mm), width: 4.00±0.13 mm, and thickness: 3.00±0.13 mm. long edges of each test specimen are chamfered/ rounded with a radius of 0.15 6 ± 0.05 mm
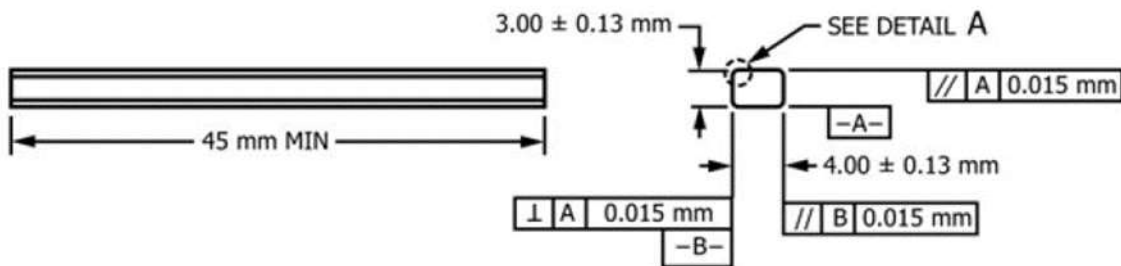

Figure 1. ASTM C1161 − 18 Standard sample dimensions "Reprinted[23]".

3.2.2.1.1. Sample configurations and zones alignments:

For achieving the objective, we created different graded and homogeneous configurations of samples, we went with stepwise gradation instead of continuous gradation as this will give us better knowledge about the impact of gradation and performance difference at each graded zone as well as overall on the sample compared to a homogeneous default sample. From the DOE we have created the following sample configurations:

1. Configuration 1: Homogeneous samples having default parameters parameter 6)

2. Configuration 2: Homogeneous samples having parameter 1

3. Configuration 3: Homogeneous samples having parameter 2

4. Configuration 4: Homogeneous samples having parameter 3

5. Configuration 5: Homogeneous samples having parameter 4

6. Configuration 6: Homogeneous samples having parameter 5

7. Configuration 7: 2 Zone graded samples having a higher hardness in outside zones and lower hardness in the core zone.

8. Configuration 8: 2 Zone graded samples having a lower hardness in outside zones and higher hardness in the core zone.

9. Configuration 9: 3 Zone graded samples having a higher hardness in outside zones, intermediate hardness in the middle zones, and lower hardness in the core zone.

10. Configuration 10: 3 Zone graded samples having a lower hardness in outside zones, intermediate hardness in the middle zones, and higher hardness in the core zone.
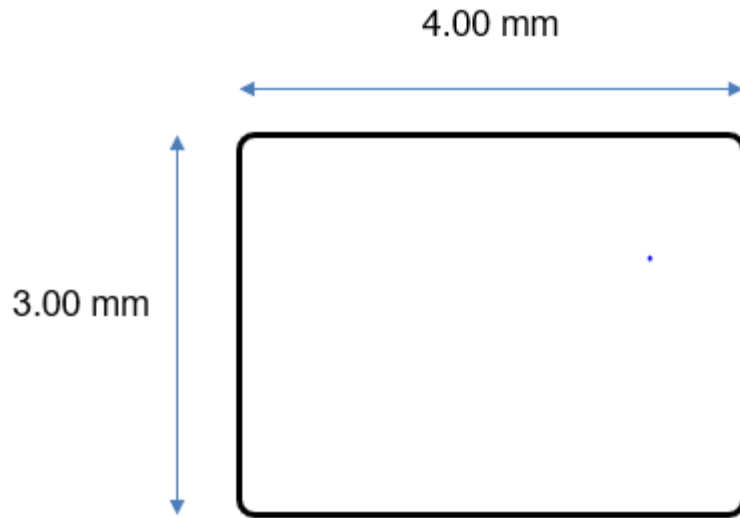
Figure 2. Cross-sectional dimensions of homogeneous samples configuration 1 to 6.
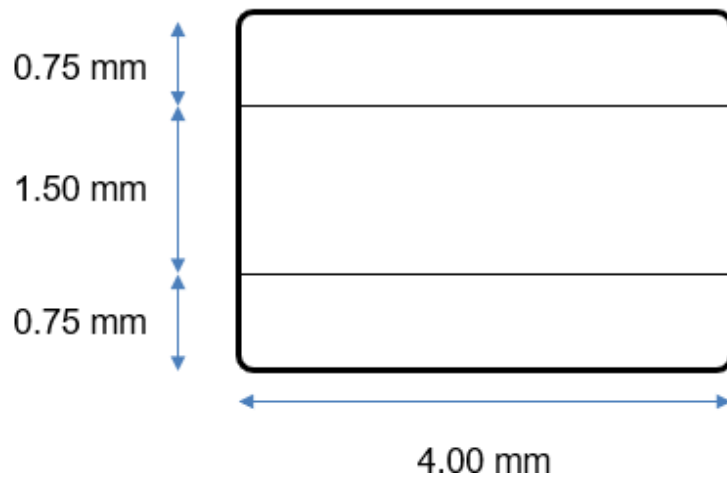

Figure 3. Cross-sectional dimensions of 2 zone graded samples configurations 7 and 8.
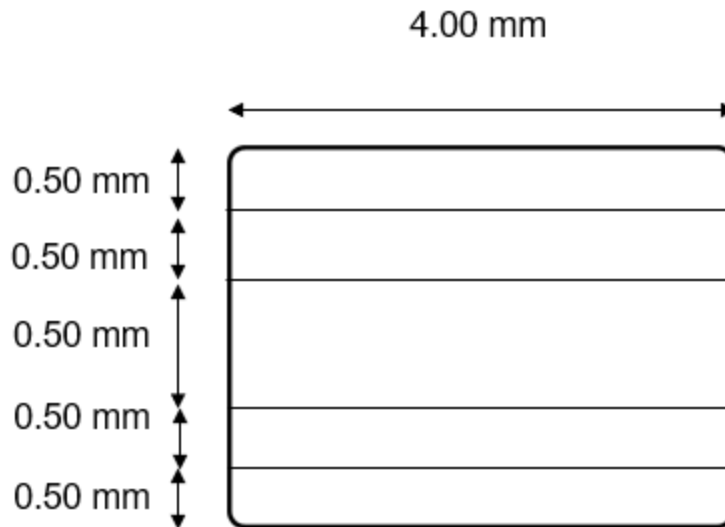
Figure 4. Cross-sectional dimensions of 3 zone graded samples configurations 9 and 10.

we selected a processing parameter to create gradation in a way so that there will be a significant difference in modulus of elasticity/hardness as possible between gradation zones within a sample. This is because of the reasoning that the higher the difference in elastic modulus/ hardness the higher the performance difference we will notice while carrying out lab experiments.

The bending samples have been tested in two sets (test set-1, and test set-2). For test set 1, to create graded samples, we selected parameter 2 (294 HV) to be the zone with higher hardness, parameter 4 (256 HV) to be the zone with lower hardness, and parameter 3 (271 HV) to be the zone having intermediate hardness.). For test set 2, to create graded samples, we selected parameter 1 (318 HV) to be the zone with higher hardness, parameter 5 (209 HV) to be the zone with lower hardness, and parameter 3 (271 HV) to be the zone having intermediate hardness.

3.2.2.2. Tensile samples:

The intention of this research was also to get a better understanding of the relationship of the elastic modulus concerning these process parameters. So, to get a proper estimation and trend of elastic modulus related to each process parameter combination we also decided to manufacture tensile samples (homogeneous) having those process parameters and perform the tensile test on them.

ASTM E8 / E8M standard has been followed to carry out the tensile tests for all the tensile samples. According to this standard, the dimensions of the samples were selected to be
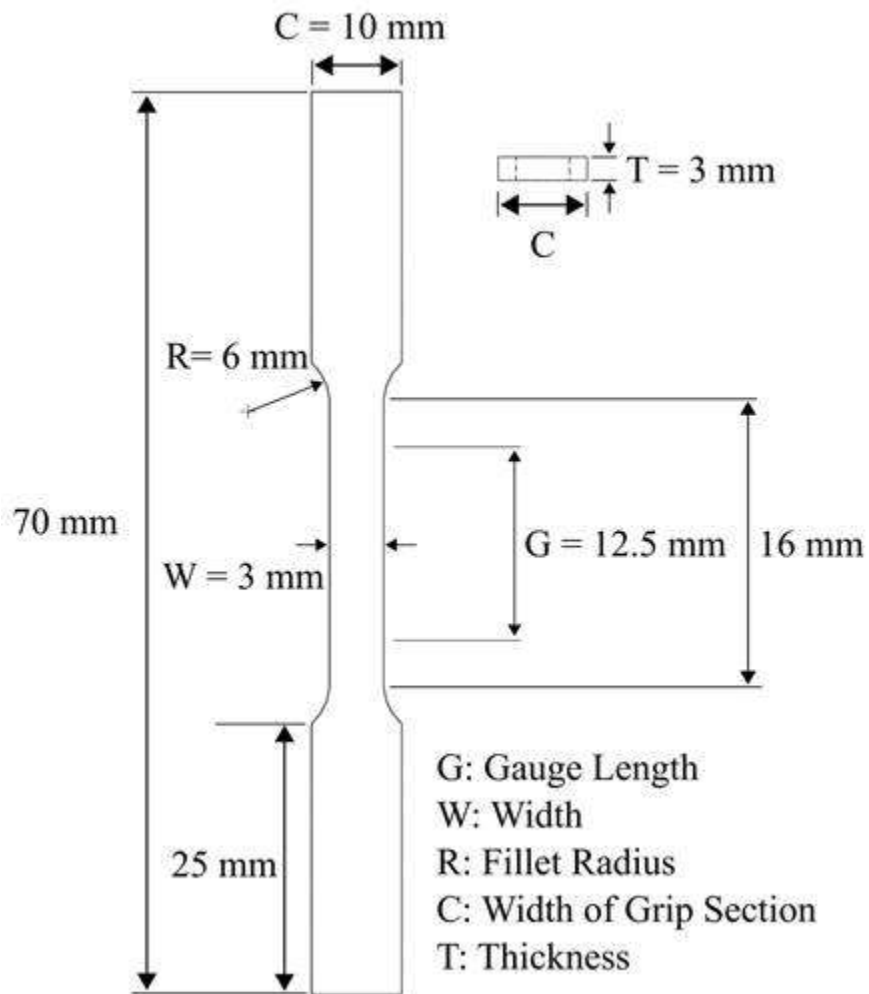

Figure 5. ASTM E8 / E8M standard tensile sample dimensions

3.2.2.2.1. Sample configurations:

1. Configuration 1: Homogeneous samples having default parameters parameter 6)

2. Configuration 2: Homogeneous samples having parameter 1

3. Configuration 3: Homogeneous samples having parameter 2

4. Configuration 4: Homogeneous samples having parameter 3

5. Configuration 5: Homogeneous samples having parameter 4

6. Configuration 6: Homogeneous samples having parameter 5

3.2.3. Modelling of samples:

Solid works 2019 was used to create CAD models of the required dimensions for both tensile and bending samples. Conversion from CAD to STL files has been done using the same software. The STL file is then imported into QuantAM software, this is the software used for creating printing profiles and selecting printing parameters for the samples.

Steps involved in creating printing file in QuantAM to import into Renishaw AM 400 machine:

1. Importing STL file into QuantAM.

2. Orientation of the model to achieve desired printing orientation of the sample.

3. Selecting and generating support, selecting material for support as well as samples.

4. Layout: create layout/arrange all the samples to be printed on the CAD model of the printing plate.

5. Select printing pattern (meander, chessboard, etc.), generate process parameter file to input process parameters for printing.

6. Review (cost, estimated printing time, etc.) and create a .mtt file that has to be imported into the machine.

After this step, the file will look like figure 13. An overview diagram of the entire manufacturing process using Renishaw AM400 has been provided in figure 14.
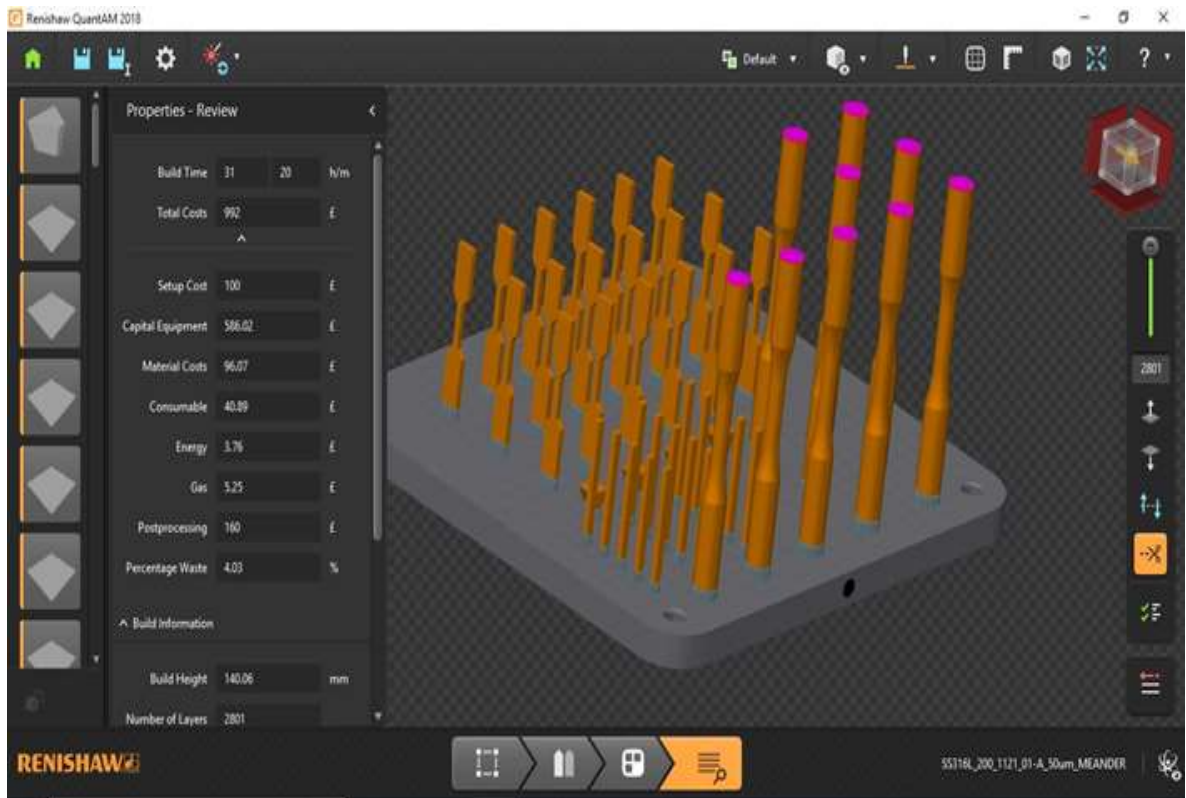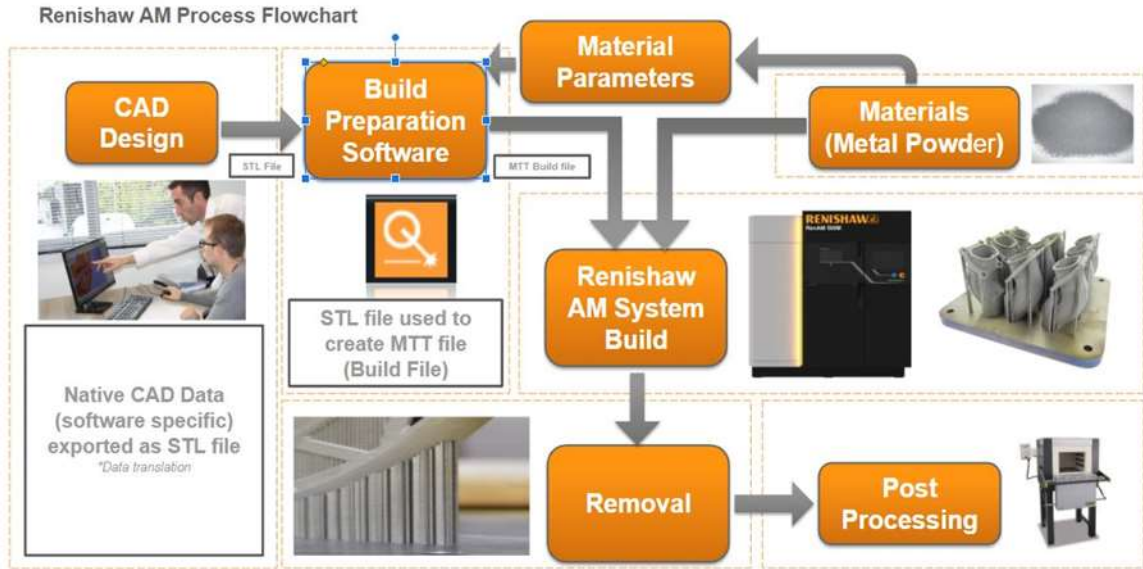

Figure 6. QuantAM CAM software interface.

Renishaw AM Process Flowchart

Figure 7. Additive manufacturing process overview using Renishaw AM400 machine.

3.2.4. Manufacturing using Renishaw AM 400:

The Renishaw AM400 metal additive manufacturing system has been used to print all the samples. This machine employs SLM to print samples layer by layer with a layer thickness of 50 microns. The printing chamber is inerted using argon gas. The chamber pressure, powder flow, and many other things can be controlled using the control panel shown in figure 16.

Figure 8. Renishaw AM400 machine

Figure 9. Renishaw AM400 control panel

The SLM process that is used to manufacture this machine is shown in figure 17.

Figure 10. SLM printing using Renishaw AM400

The printed samples can be seen in figure 18. The left side image in that figure shows the bending sample. The gradation zones can be seen in the enlarged image. The right-side image in the figure shows the different types of samples printed including tensile, bending, and fatigue samples.
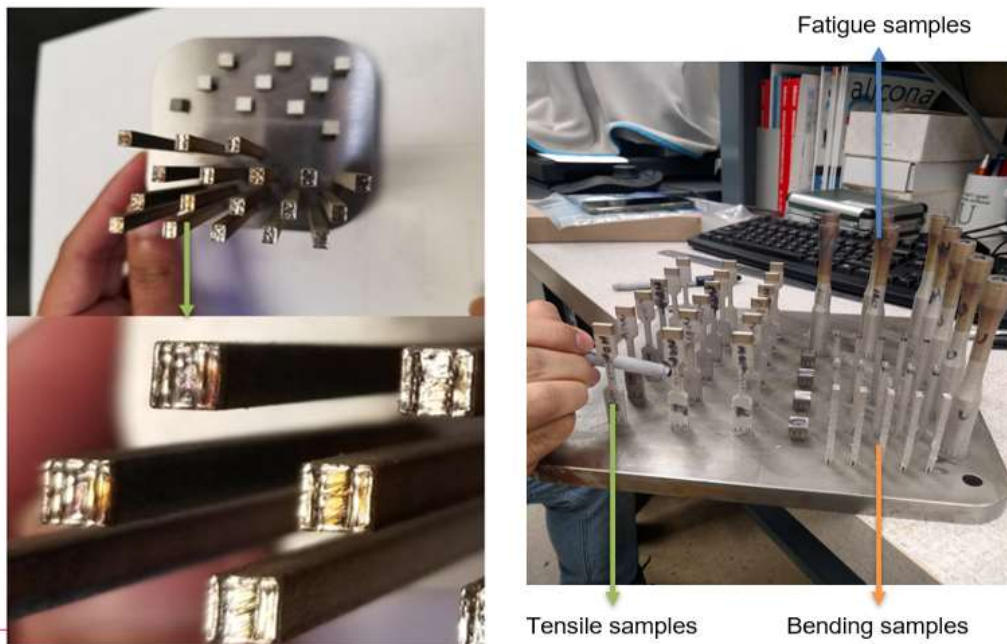

Figure 11. manufactured samples

3.2.5. DIC implementation and speckling

One of the objectives of this research is to monitor and determine the strain profile and deformation behavior of all the bending samples. For this, a 2D Digital image correlation (DIC) was used to monitor the surface deformation during all the experiments. For incorporating DIC certain steps are involved which are:

- Speckling the samples with contrasting patterns

- Setting up the camera and lighting source accurately to capture highly detailed images.

- Using DIC camera software to capture images at a certain rate.

- Collecting all the images and analyzing them using DIC software.

- Postprocessing of the DIC analysis (includes strain and deformation calculations).

- Generating output plots for different pixels.

All the samples are initially painted with white paint, then the DIC speckling kit is utilized to create a certain contrasting pattern on the samples. The kit can be seen in the left side image of figure 19. The kit contains an ink pad and many rollers with different sizes of teeth.

An appropriate-sized roller is selected, and the ink is applied on the roller from the ink pad. Then the roller is rolled over the white painted sample surface to make the speckling pattern.

Figure 12. DIC speckling kit and speckled samples

The DIC camera and lighting setup are done to achieve highly detailed images of the sample throughout the experiment. The camera and lighting setup are shown in figure 20.

Figure 13. Camera and Lighting setup for DIC.

The DIC software is used to control the camera settings like rate of taking images, focus, zoom, etc. for these experiments the rate at which images are taken is 1 image every 2 seconds. Each sample

generated around 270 images that were processed and the results and plots have been presented in the

result and analysis section (chapter 4).

RESULTS AND ANALYSIS

4.1. Experiments and results:

4.1.1. Tensile tests:

The tensile test was carried out to estimate the elastic behavior of all the tensile configurations discussed in section 3.2.2.2.1. and understand the trend of performance of all the configurations. A total of 18 samples were tested that consist of 6 different configurations (listed in table 6). having 3 repetitions each. The MTS Exceed model E44 universal tensile testing machine has been used to perform all the tensile tests.

The ASTM E8 / E8M standard has been followed to carry out all the testing procedures and conditions. According to this standard, the crosshead speed was maintained at a constant rate of 1.0 mm/min to achieve the suggested strain rate.

Table 6. Tensile Sample configurations

Number	Power P [W]	Exposure Time T [µs]	Hardness [HV.5]	E (Nano Elastic modulus) (GPa)
Homogeneous sample 1	200	74	318±2.4	162.99±2.95
Homogeneous sample 2	150	63	294±6.1	154.09±7.38
Homogeneous sample 3	200	68	271±5.8	187.48±7.30
Homogeneous sample 4	200	92	256±9.6	211.03±12.67
Homogeneous sample 5	175	63	209±4.7	203.92±6.08
Homogeneous sample 6	200	80	261±2.4	197±4

4.1.1.1. Stress vs strain of the fabricated tensile samples:

The general stress vs strain plot for all the samples will look like figure 21. The loading starts at a rate of 1mm/ minute and then when the strain reaches 0.2 % unloading occurs at the same rate till load becomes 0 N, then the loading is applied at the same rate till it reaches 2% strain. The unloading is done at that point till the load becomes 50 N. once it reaches that load the loading is applied till the fracture point. Throughout the process, the loading and unloading rate is kept constant at 1.0 mm/min. the loading and unloading cycles are done in 0.2 % and 2 % strain to obtain the loading and unloading elastic modulus of each sample.
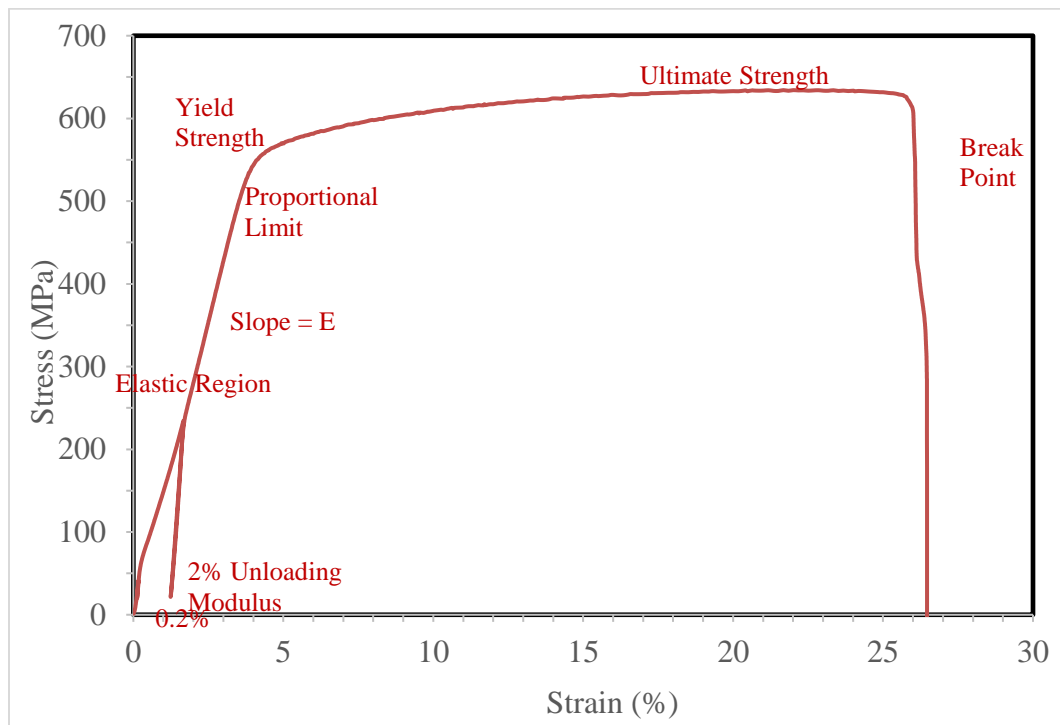
Figure 14. Representative stress vs strain plot for one of the samples.

The stress vs strain is plotted for all 3 reputations of homogeneous sample 1 (HV 318). Homogeneous sample 1 (318-2) and Homogeneous sample 1 (318-3) showed similar slopes in the elastic zone but Homogeneous sample 1 (318-1) behaved significantly differently in the same region. In

the plastic regime, the behavior was not repeated for any sample. All 3 reputation samples showed very different behavior in terms of peak stress, peak strain, and strain at the point of failure. All these can be observed from figure 22.
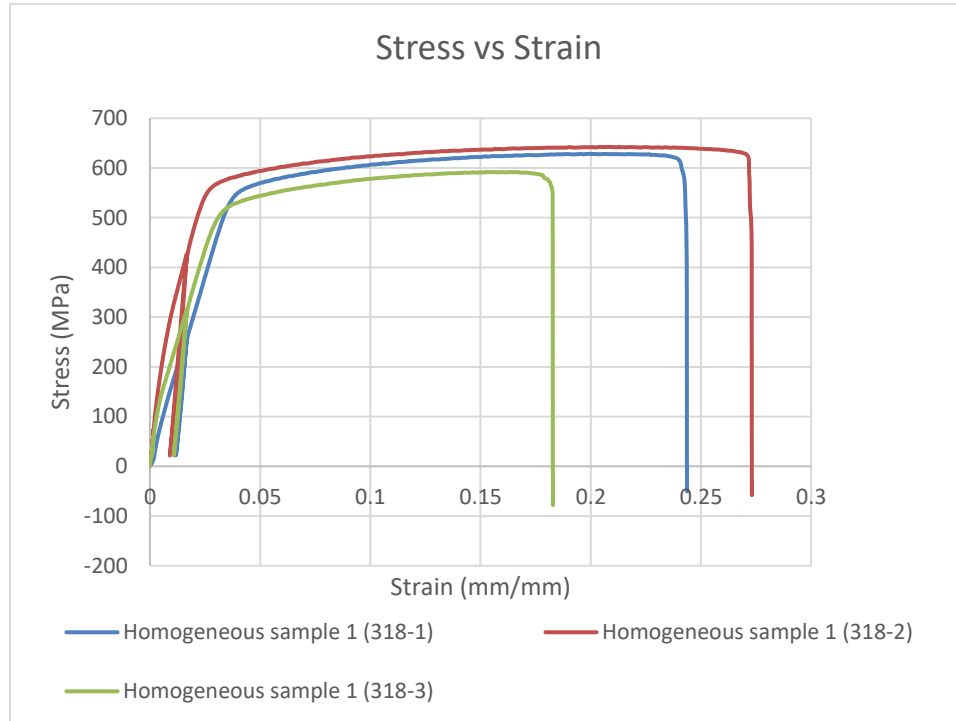

Figure 15. Stress vs strain for Homogeneous sample 1

The stress vs strain is plotted for all 3 reputations of homogeneous sample 2 (HV 294). As seen from figure 23, Repetition 1 and 3 showed similar behavior but 2 showed significantly different behavior in the elastic regime. Plastic behavior was different for all the 3 repetition samples.
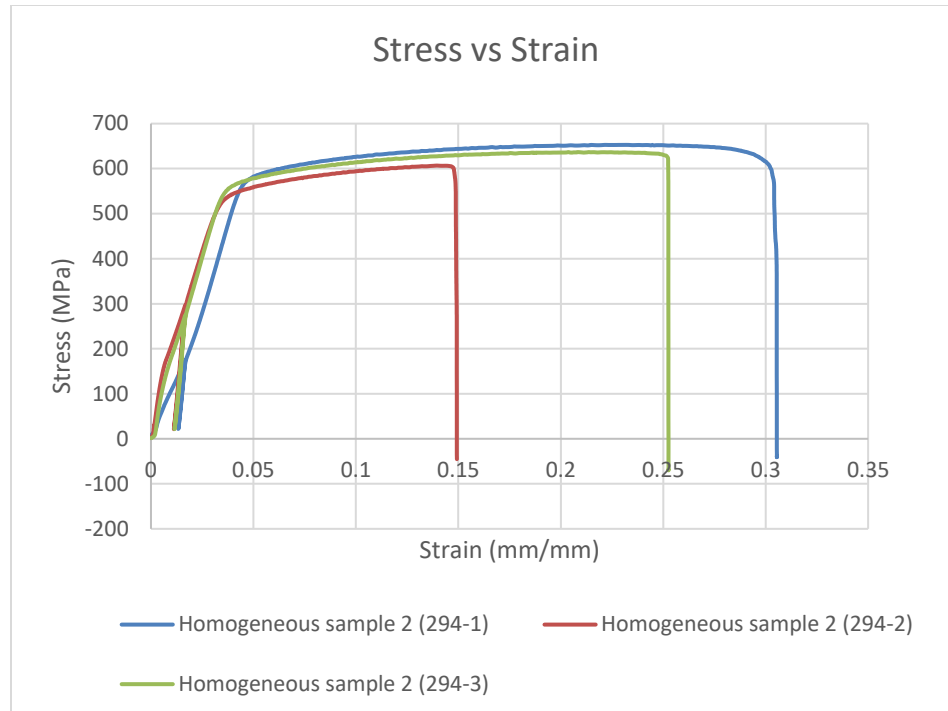
Figure 16. Stress vs strain for Homogeneous sample 2

The stress vs strain is plotted for all 3 reputations of homogeneous sample 3 (HV 271). All 3 samples in this configuration showed very good repeatability in the elastic range. But in the plastic range sample, no-3 of this configuration failed very early compared to the other 2 samples. The other 2 samples i.e., sample no- 1 and 2 showed very similar behavior in the plastic range as well which can be seen from figure 24.
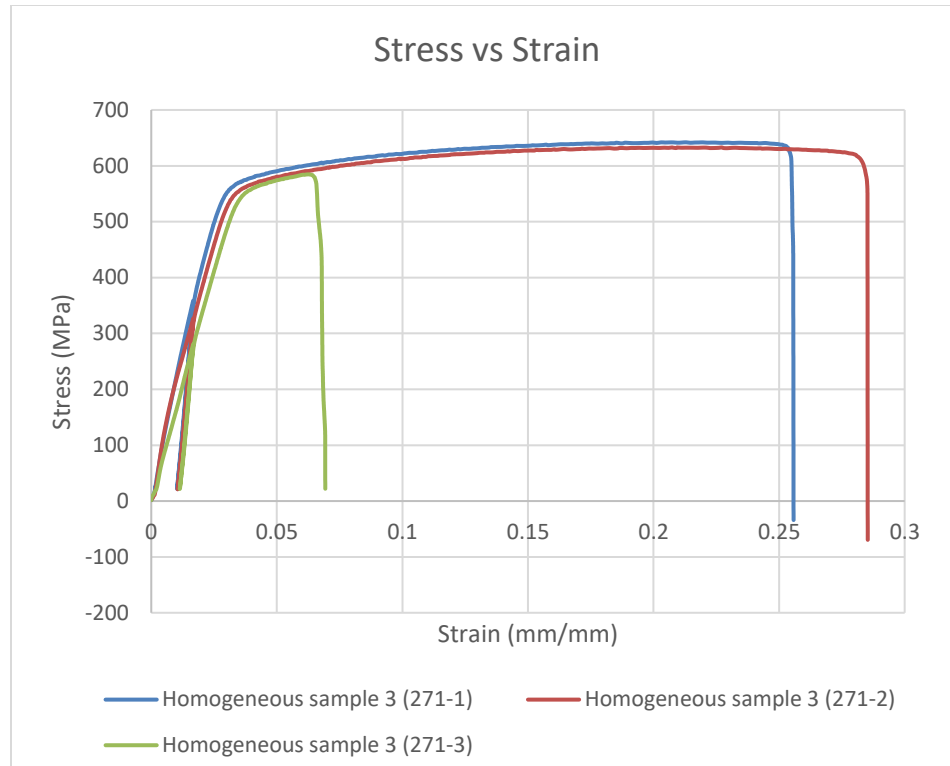
Figure 17. Stress vs strain for Homogeneous sample 3

The stress vs strain is plotted for all 3 reputations of homogeneous sample 4 (HV 256) seen in figure 25. Sample no-1 and 2 in this configuration showed very good repeatability in the elastic as well as plastic zones but sample-3 failed fairly early while undergoing plastic deformation as a result even though it showed good repeatability in the elastic zone its plastic behavior is not repeated as compared to other two samples in this configuration.
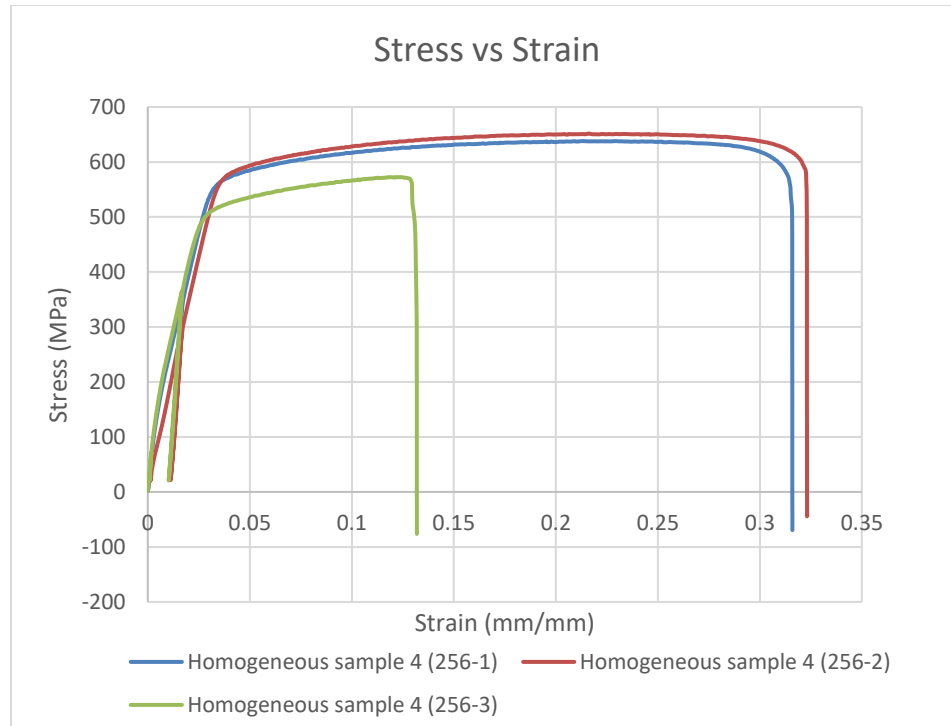
Figure 18. Stress vs strain for Homogeneous sample 4

The stress vs strain is plotted for all 3 reputations of homogeneous sample 5 (HV 209) as seen in figure 26. For this configuration, all 3 repeated samples showed good repeatability in both elastic and plastic regimes.
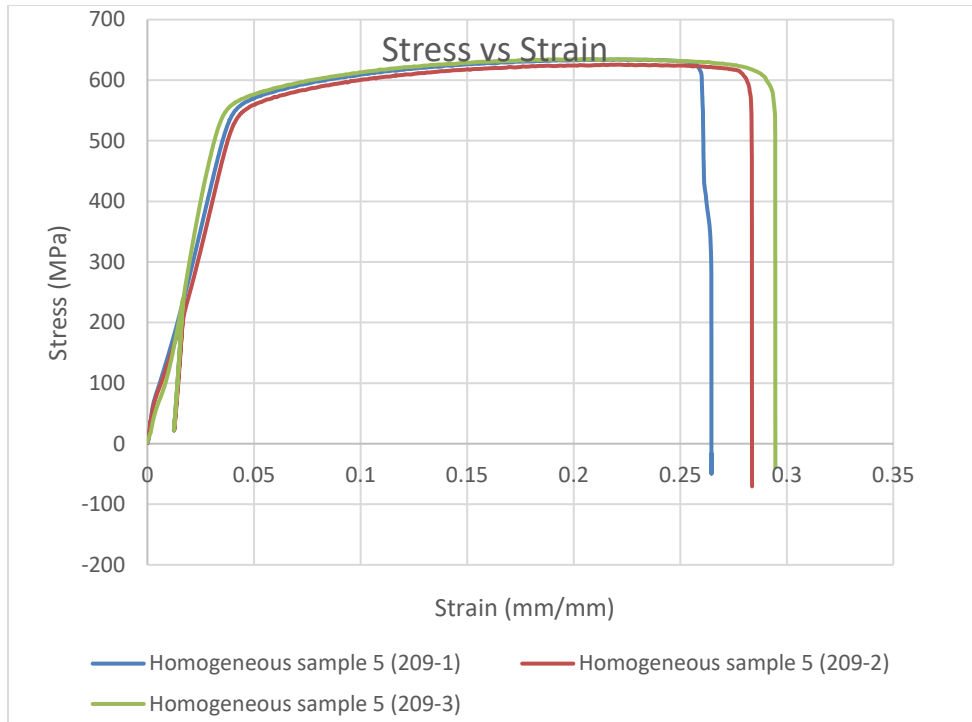
Figure 19. Stress vs strain for Homogeneous sample 5

The stress vs strain is plotted for all 3 reputations of homogeneous sample 6 (HV 261). As evident from figure 17. All 3 samples showed good repeatability in the elastic zone and to some extent in the plastic zone. But sample-3 in this configuration failed pretty early, sample 2 also failed early though not as quickly as sample-3. Sample-1 sustained the plastic deformation the longest.
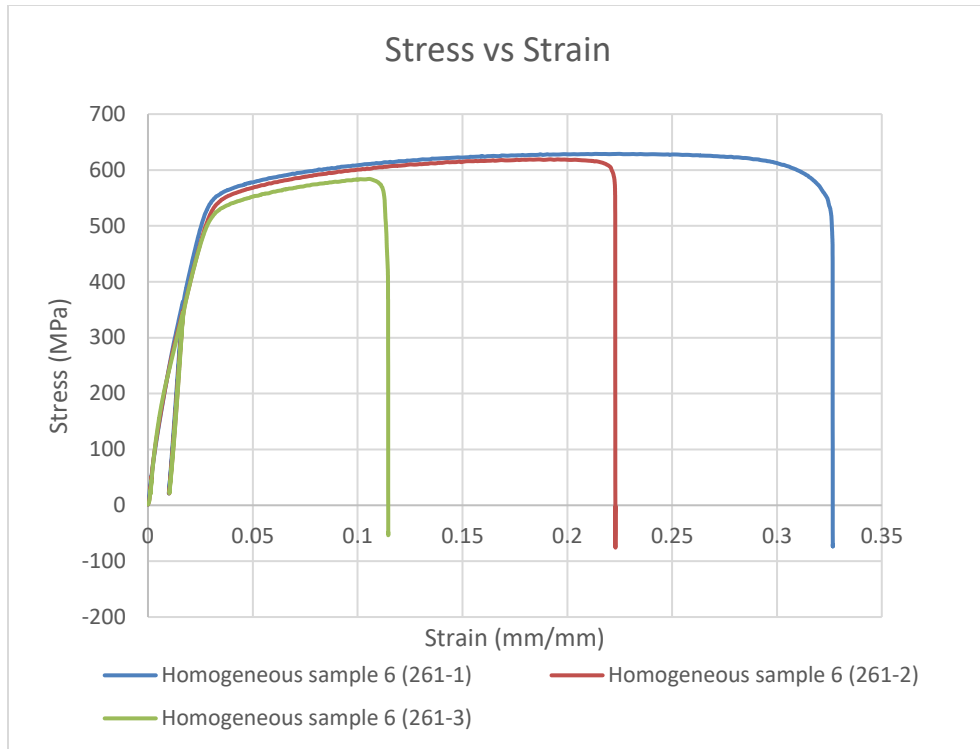
Figure 20. Stress vs strain for Homogeneous sample 6

Load vs displacement comparison between all the configurations and plotted in figure 28. Our expectation before the experiment was that samples with lower expected hardness should have a lower slope compared to samples with higher expected hardness. That expectation was not matched. Our expectation was based on the assumption that microhardness and elastic modulus are proportionally related but that is not the case as proven by the experimental data.
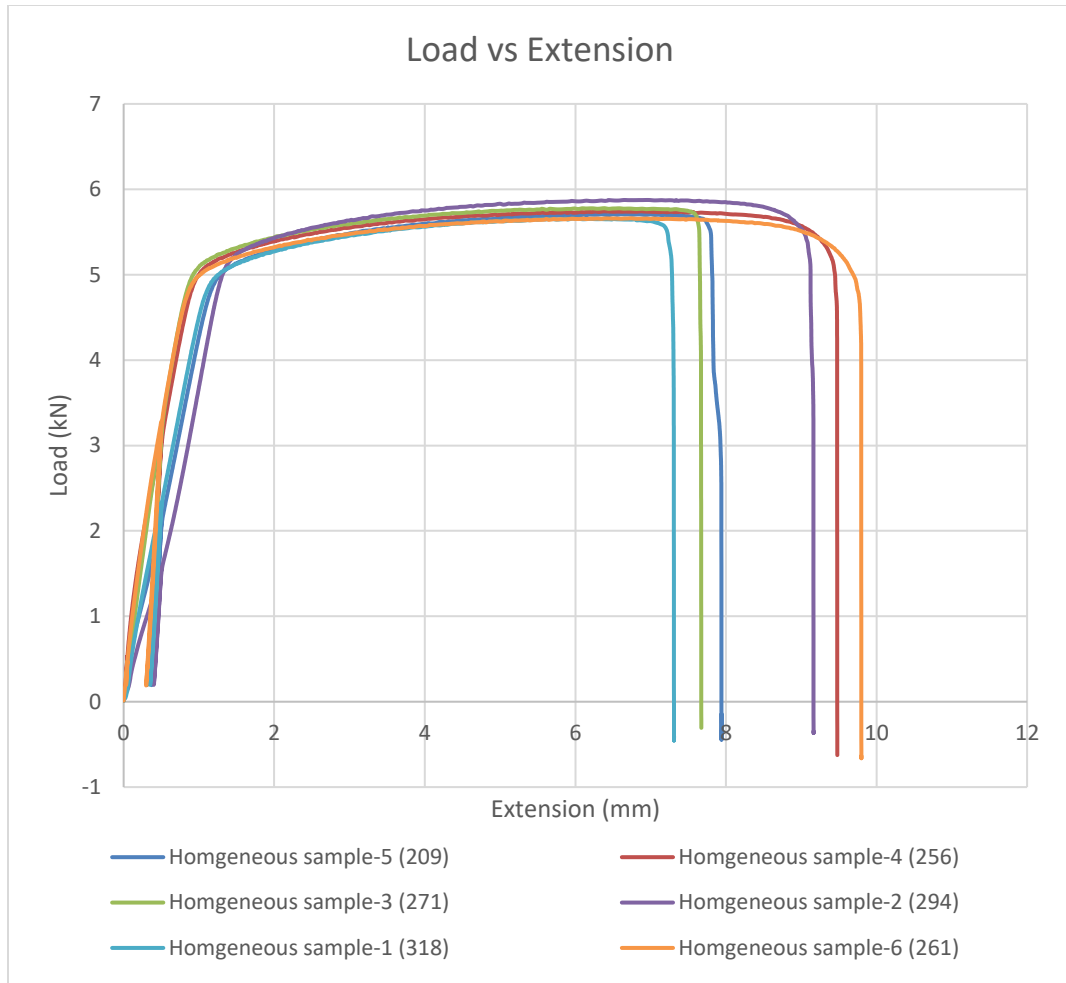
Figure 21. Averaged Load vs Deflection comparison plot for all homogeneous configurations

The peak load and strain at the breakpoint for all the samples have been presented in table 7.

Table 7. Peak load and strain at breakpoints for all configurations

Sample configuration	Peak Load (kN)	Average Peak Load (kN)	Strain at Break (mm/mm)	Average Strain at Break (mm/mm)
Homogeneous sample-5 (209-1)	5.708	5.69±0.04	0.26	0.262±0.008

Table 7 Continued

Sample configuration	Peak Load (kN)	Average Peak Load (kN)	Strain at Break (mm/mm)	Average Strain at Break (mm/mm)
Homogeneous sample-5 (209-2)	5.635		0.271	
Homogeneous sample-5 (209-3)	5.715		0.256	
Homogeneous sample-4 (256-1)	5.742	5.59±0.38	0.279	0.237±0.079
Homogeneous sample-4 (256-2)	5.864		0.287	
Homogeneous sample-4 (256-3)	5.152		0.146	
Homogeneous sample-3 (271-1)	5.779	5.58±0.28	0.256	0.194±0.103
Homogeneous sample-3 (271-2)	5.696		0.251	
Homogeneous sample-3 (271-3)	5.263		0.075	
Homogeneous sample-2 (294-1)	5.875	5.69±0.21	0.266	0.230±0.054
Homogeneous sample-2 (294-2)	5.461		0.168	
Homogeneous sample-2 (294-3)	5.731		0.256	
Homogeneous sample-1 (318-1)	5.656	5.69±0.24	0.235	0.227±0.033
Homogeneous sample-1 (318-2)	5.785		0.255	
Homogeneous sample-1 (318-2)	5.326		0.191	
Homogeneous sample-6 (261-1)	5.66	5.50±0.21	0.292	0.216±0.083
Homogeneous sample-6 (261-2)	5.572		0.23	
Homogeneous sample-6 (261-3)	5.257		0.127	

The average elastic modulus in the elastic regime (stress associated with 2% strain to around 600 MPa) is calculated and presented in table 8.

Table 8. Average elastic modulus at 2% strain for all configurations

sample	E (2% Strain)	Average
209 F	15.51	14.20
209 M	14.20	
209 B	12.88	
318 F	16.41	25.33
318 M	35.05	
318 B	24.54	
260 F	25.33	25.66
260 M	25.65	
260 B	26.01	
294 F	10.71	17.07
294 M	22.38	
294 B	18.13	
271 F	22.25	20.24
271 M	21.95	
271 B	16.52	
256 F	26.39	24.33
256 M	17.68	
256 B	28.92	

4.1.2.1. Bending test set 1

All the bending tests have been carried out in two sets, bending test set-1 and bending test set-2. The detailed results of the bending test set-2 have been discussed in this section. In this test set, 15 samples have been tested. These 15 samples comprise of 3 different configurations each having 5 repeated samples. The 3 different configurations are listed in table 9. The machine that has been used for carrying out all the tests in this test set is MTS Exceed Model E44. The bending test type is a displacement control with a displacement cutoff of 2.5 mm at the loading points in the transverse direction. According to the ASTM standard that has been followed for the test the strain rate has to be maintained at $1.0 \times 10^{-4}s^{-1}$. To achieve this strain rate for our sample size the crosshead speed was determined to be 0.50 mm/min.

Table 9. Test set-2 bending sample configurations.

Sample configurations	Power (W)	Exp time(μs)	Microhardness (HV)	Elastic modulus (GPa)
Homogeneous	200	80	261	25
2 Zone out high	200/175	74/63	318/209	24*
2 Zone out low	175/200	63/74	209/318	16*

Load vs deflection plot is generated for all five repeated homogeneous samples (seen in figure 29). All 5 samples have a very similar slope and curvature, bulk/global performance is very consistent

for all the samples. repeatability is good suggesting consistent testing procedure and condition. It also says that there isn't any significant manufacturing defect that can alter the bulk behavior of any of the five repeated samples. The elastic region is expected to be around 50 N to 600 N.
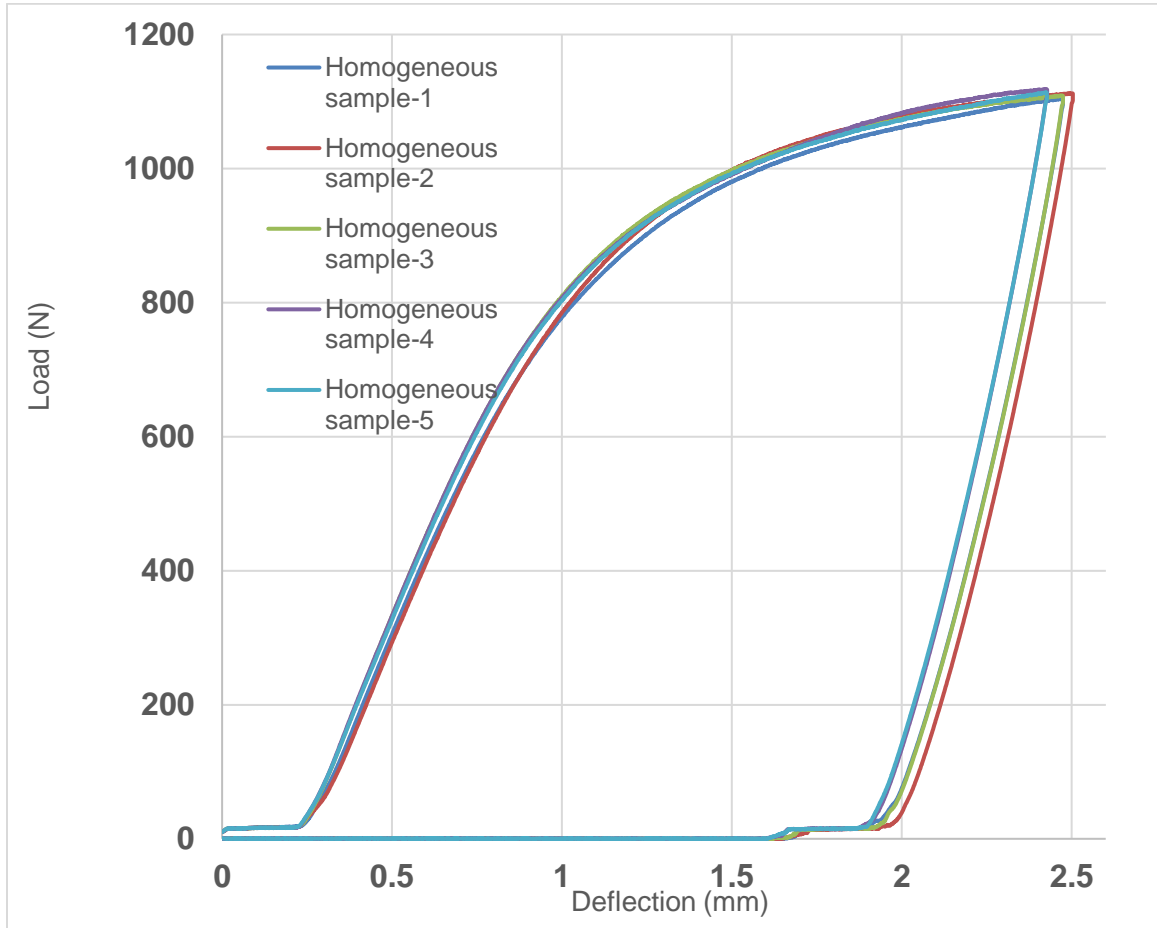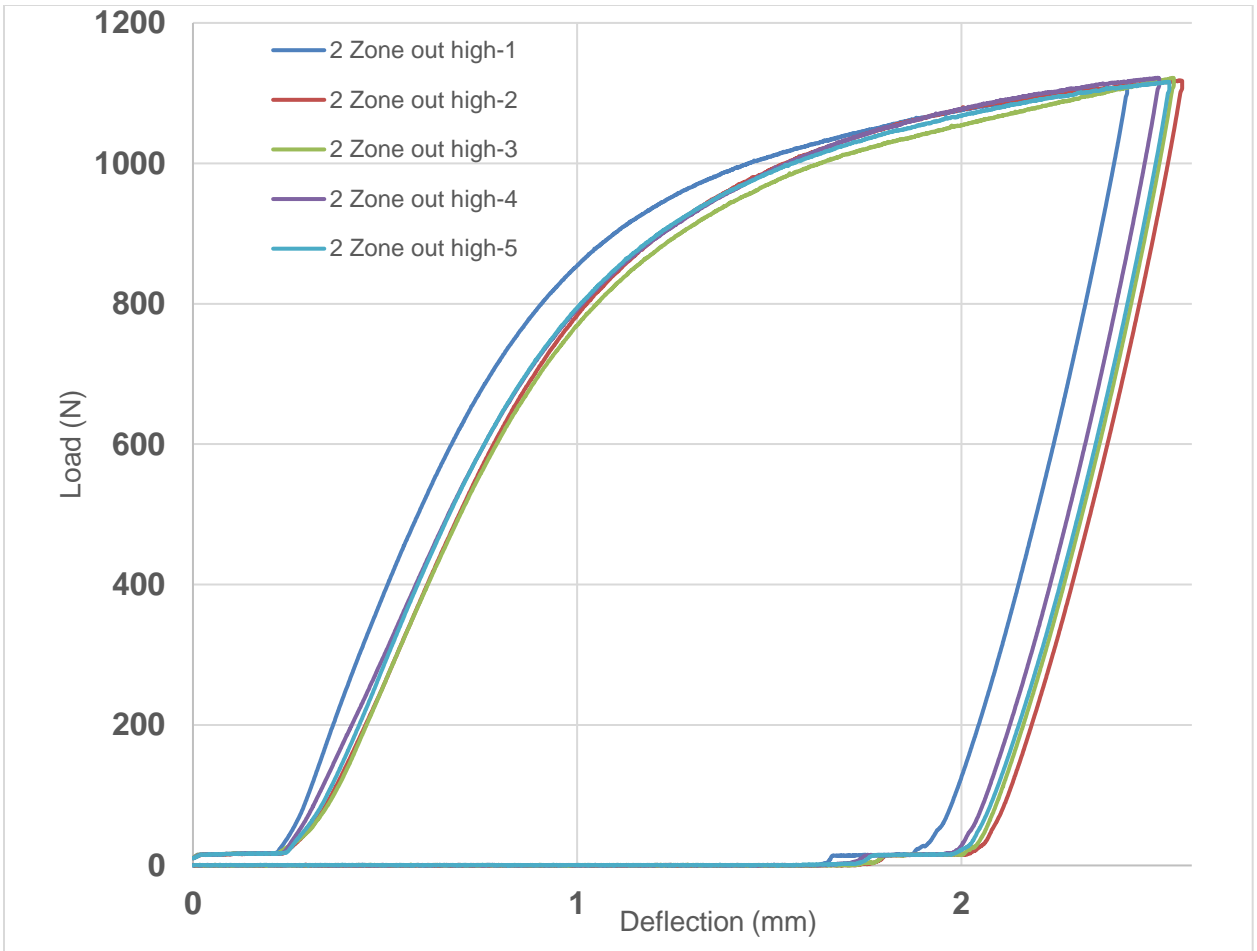

Figure 22. Load vs Deflection plots for homogeneous samples

Load vs deflection plot is generated for all five repeated 2 Zone out high samples as seen in figure 30. 2 Zone out high sample-1 is not following the normal trend unlike other 4. That can be called an abnormality or outlier. This abnormality might have been caused by any manufacturing issue.

Figure 23. Load vs Deflection plots for 2 zones out high samples

Load vs deflection plot is generated for all five repeated 2 Zone out low samples. sample-5 of this configuration is not following the normal trend as seen in figure 31, hence can be called an outlier, this might be due to some manufacturing defects within the sample or some alteration during the laser melting phase of the manufacturing.
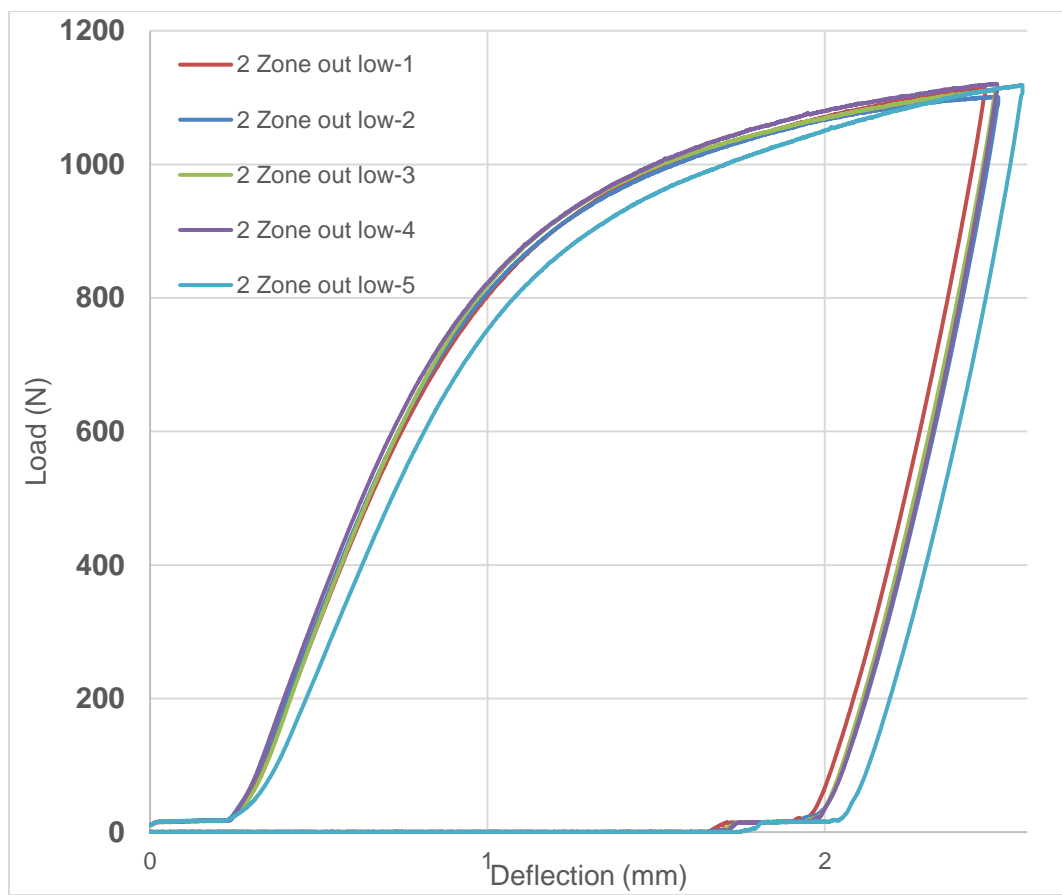

Figure 24. Load vs Deflection plots for 2 zones out low samples

The load and deflection corresponding to the load for all the samples in each configuration were averaged out by excluding the outliers and then load vs deflection plots have been compared against other configurations (figure 32).
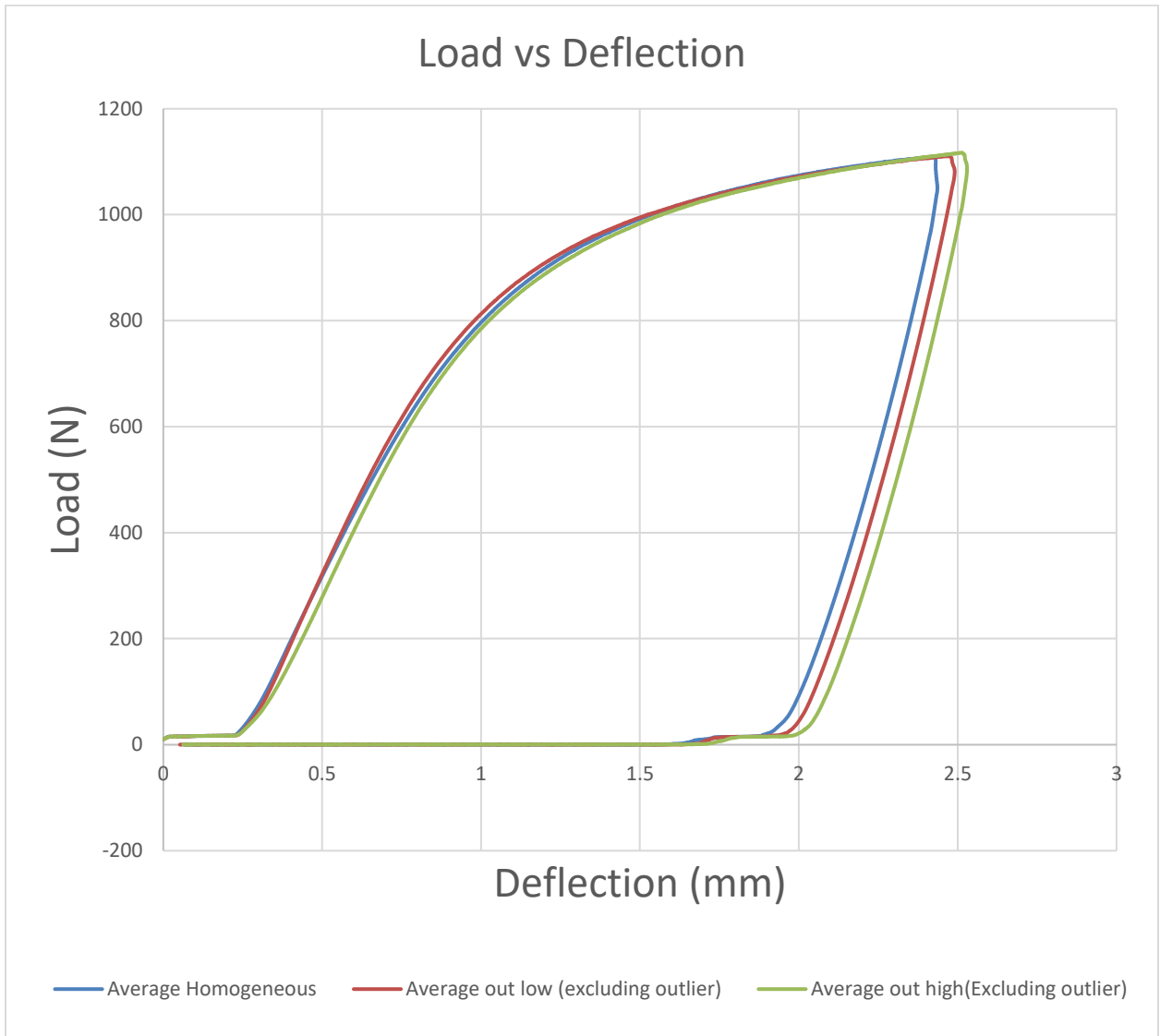

Figure 25. Load vs Deflection comparison between three configurations

The expected trend in terms of the slope is that graded samples having a higher hardness value on the outside should have a higher slope than the other two configurations (under the assumption that hardness value is proportional to elastic modulus). Graded samples having lower hardness on the outside

should have the least slope. That expectation is not followed in the plot where the out high sample has

the least slope, and the out low sample and homogeneous samples have almost similar slope.

This behavior is defying our expectations. From this, we believe that hardness value not

necessarily relates proportionally to elastic modulus and there might be some samples that have higher

hardness with lower elastic modulus compared to other samples having lower hardness but higher elastic

modulus.

4.1.2.2. Bending test set 2.

The bending test set-1 had 18 samples that had been tested to obtain the mechanical performance

under flexural bending. 10 different sample configurations (listed in table 10) have been tested in this

test set. Those configurations have six homogeneous samples each having different processing

parameters mentioned in the DOE table (parameter 1 to 6), four 2 Zone out high samples, four 2 Zone

out low samples, two 3 Zone out high samples, two 3 Zone out low samples. MTS Insight

Electromechanical Testing system has been used to carry all the tests in this test set. The strain rate is

kept at $1.0 \times 10{-}4s{-}1$ by keeping a constant crosshead speed of 0.5 mm/min. DIC has been

implemented for all the samples tested in this test set.

Table 10. The bending test set 1 sample configurations.

Sample configurations	Power (W)	Exp time(µs)	Micro hardness (HV)
Homogeneous sample 1	200	74	318
Homogeneous sample 2	150	63	294
Homogeneous sample 3	200	68	271
Homogeneous sample 4	200	92	256

Table 10 continued

Sample configurations	Power (W)	Exp time(μs)	Micro hardness (HV)
Homogeneous sample 5	175	63	209
Homogeneous sample 6	200	80	261
2 Zone out high	150/200	63/92	294/256
2 Zone out low	200/150	92/63	256/294

Load vs defection for all 6 homogeneous sample configurations (6 different parameters set) has been plotted in figure 33. Sample-6 showed an extremely high slope which was not expected.   Sample 2 had the second-highest slope in the elastic region. The other 4 configurations showed a very similar slope pattern.
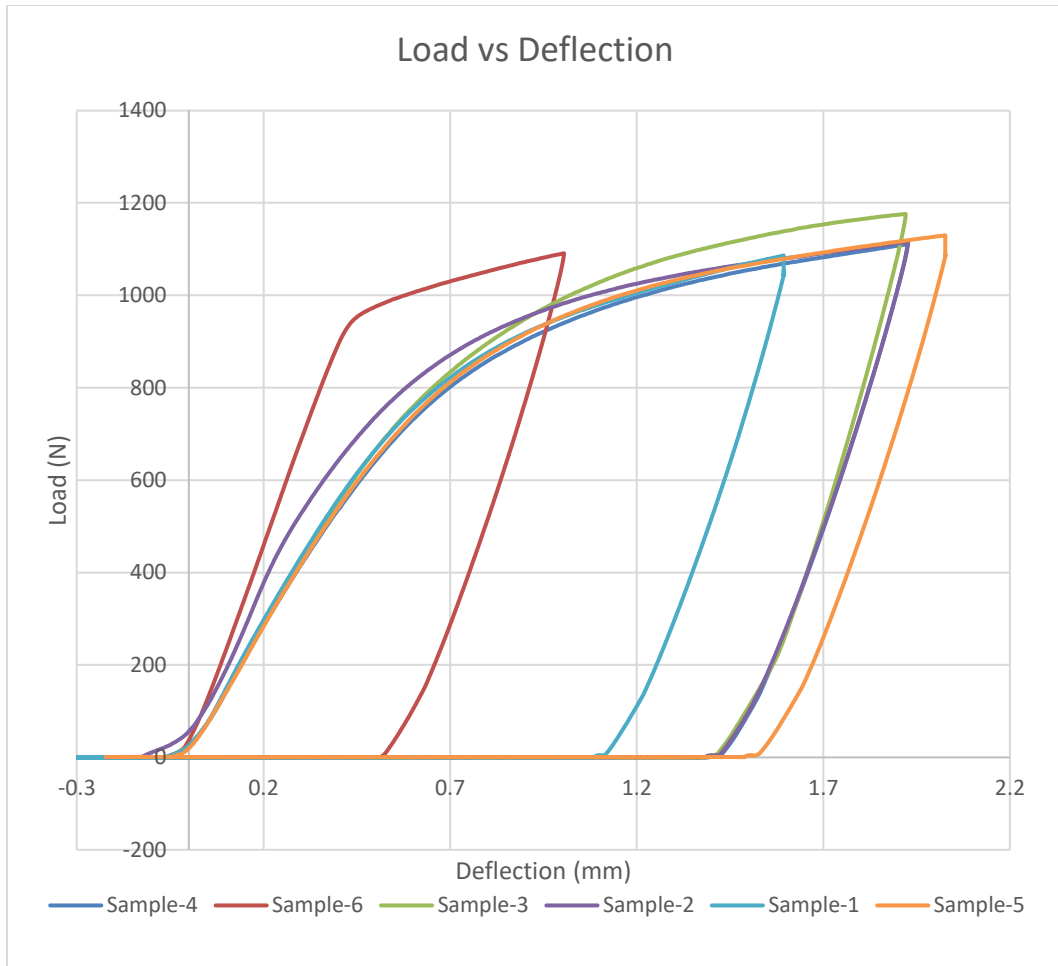
Figure 26. Load vs Deflection comparison for all 6 homogeneous sample configurations

54

Load vs deflection for all 4 repeated samples of two-zone out low (out 256HV in 294 HV) have been plotted as seen in figure 34. Repetition-1 has the highest slope and repetition-2 has the lowest slope. The other two samples in this configuration have similar slopes and behavior.
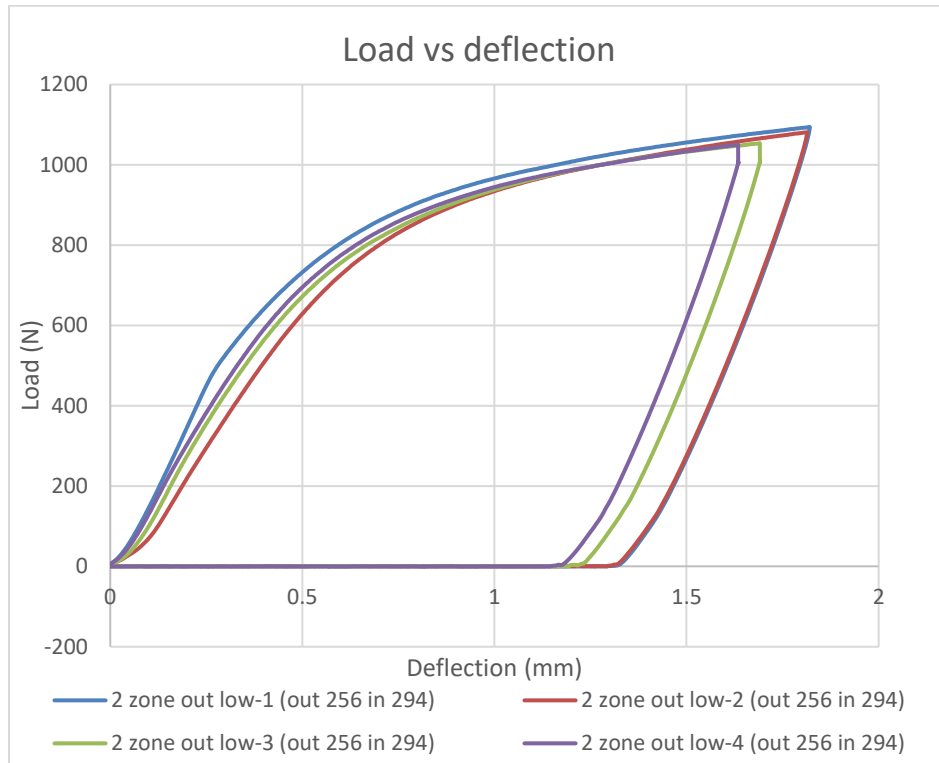

Figure 27. Load vs Deflection plot for two-zone out low samples

Load vs deflection for all 4 repeated samples of two-zone out high (out 294HV in 256 HV) have been plotted in figure 35. All 4 repetitions showed a very similar trend in both elastic and plastic regions.
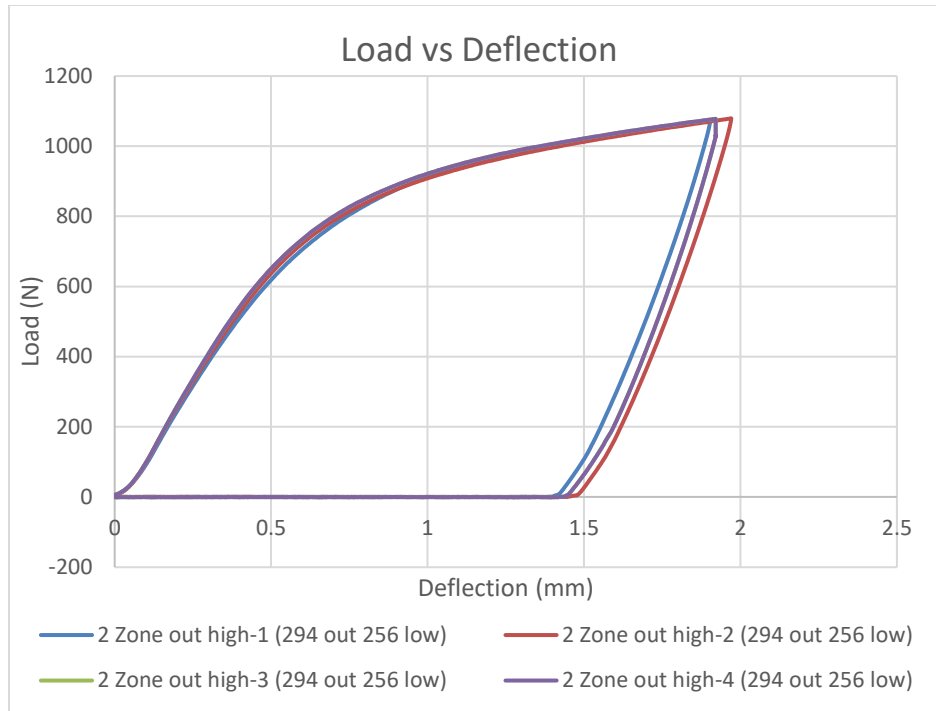
Figure 28. Load vs Deflection plot for two-zone out high samples

Load vs deflection comparison between 2 zones out low, 2 zones out high samples,
homogeneous sample 2 (HV 294), and homogeneous sample 4 (HV 256) have been presented in
figure 36. Our expectation was that sample homogeneous sample 2 (HV 294) will have the highest
slope than 2 zones out high, then 2 zones out low, and homogeneous sample 4 will have the least
slope. The expectation was not met when comparison was done. 2 zones out low sample had the
highest slope followed by 2 zones out high, homogeneous sample-4, and homogeneous sample-2
respectively. In this set of experiments, I did not manufacture any repeatable sample for
homogeneous configurations 1-6. Hence this behavior cannot be considered with full confidence. To
avoid such ambiguity, we performed bending test set-2 which has been discussed at the very
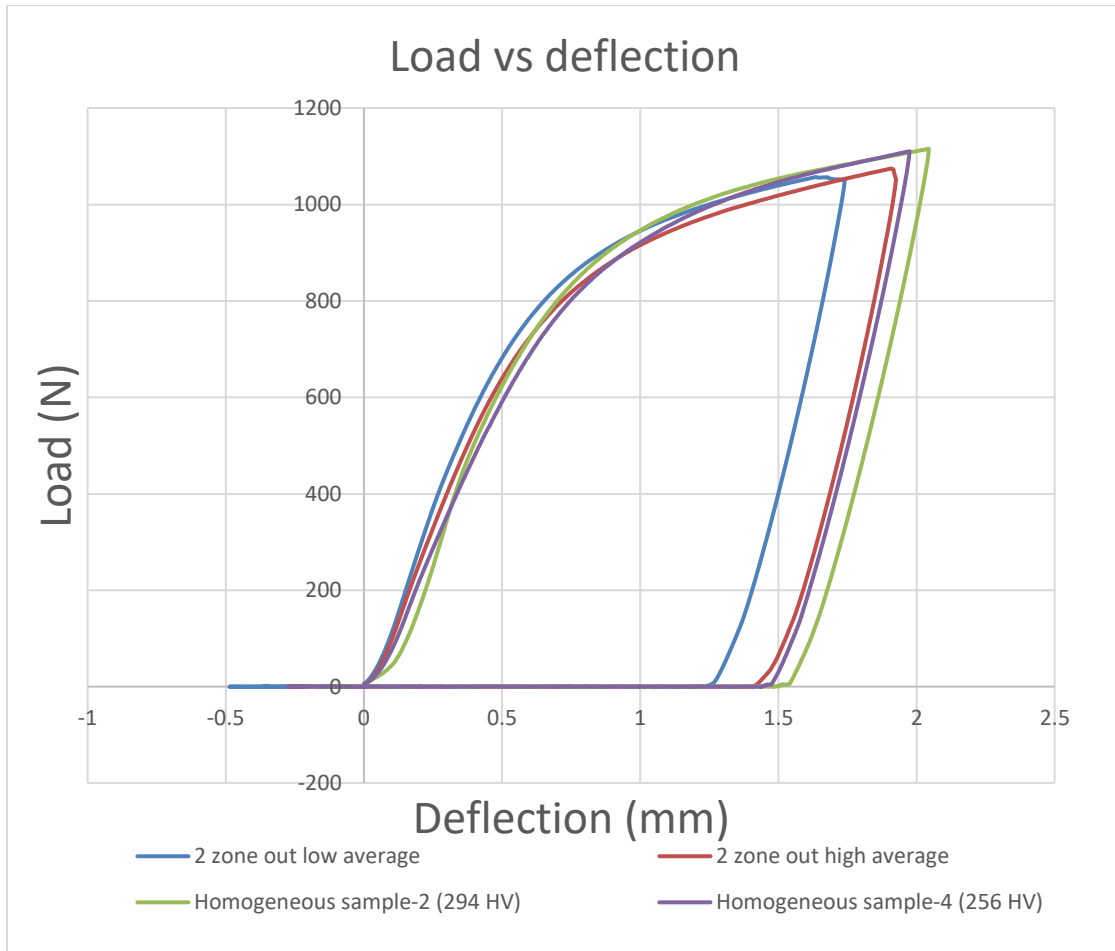beginning of section 3.1.2. of this chapter.

Figure 29. Comparison between 2 zones out low, 2 zone out high samples, and homogeneous samples:

4.1.3. DIC Analysis:

DIC images were analyzed for all the samples. The most relevant homogeneous samples were homogeneous sample 2 and homogeneous sample-4 since the parameters that have been used for printing these samples have also been used for creating gradation in the functionally graded samples.

4.1.3.1. Homogeneous sample -2 (294 HV):

The strain profile for some lines and points in the region of interest (ROI) was selected by carefully counting the pixels to make the data obtained consistent for all the samples. For a line (L0) that

spans the entire thickness of the sample and in the center of the sample along its length, the strain profile in x-direction looked like figure 37. ROI is the green region in the figure.
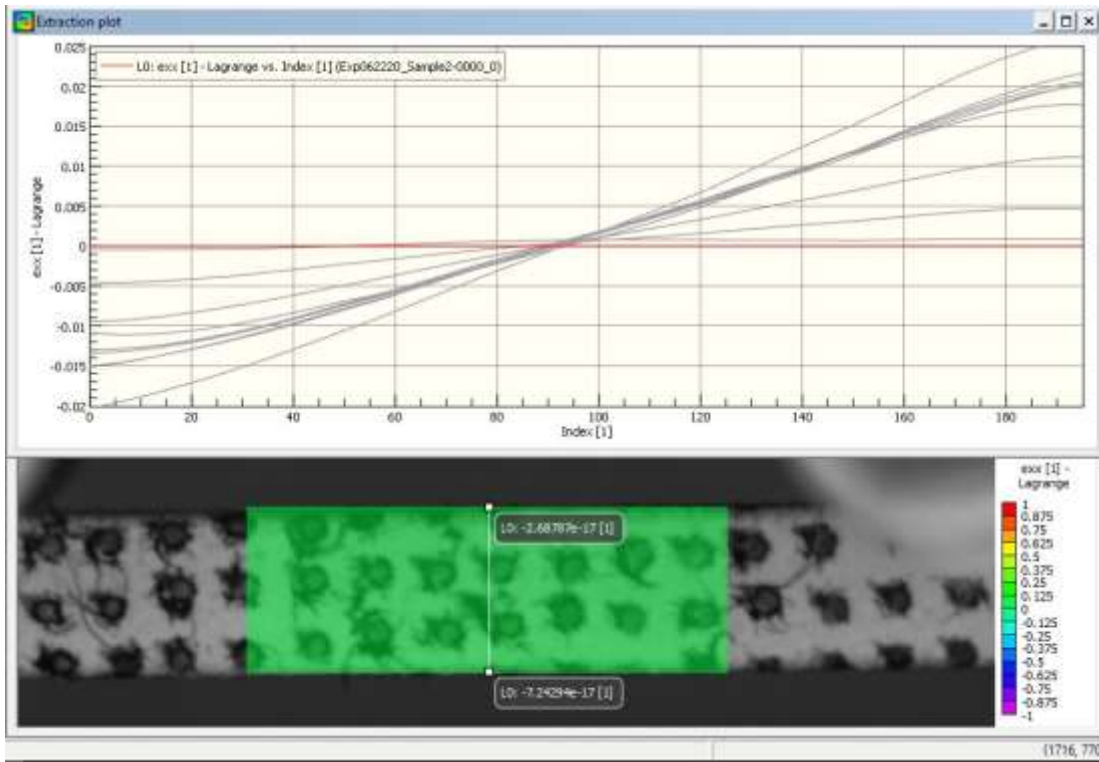

Figure 30. Strain profile in X-direction for a line L0 in Homogeneous sample -2

In this figure the X-axis represents the length of the line consisting of 200 pixels points across the thickness of the sample (i.e. top point of the line is 0th pixel and bottom point on the line is 200th pixel), Each line is an instant of time (total 276 lines for 276 images but few are identifiable from naked eye), and Y-axis represents strain value.

The strain (E_{xx}) is almost 0 at time 0 as seen in the figure (the red line), the neutral axis is at around pixel no. 90 where strain along the x-direction is always zero. The pixel points above the neutral axis (0-90) undergo gradual compression and below the neutral axis (90-200) undergo gradual tension when subjected to incremental flexural loading. The asymmetry in the plot is due to the manual

58

inaccuracy involved in locating the neutral axis point along the line L0. All this DIC information is matching or expectation.

The strain profile along the Y-direction also follows a similar pattern except that the lines are not straight instead those are parabolic curves as shown in figure 38. This is most likely due to the sample not being a very thin beam (d/L is not very small/ negligible)
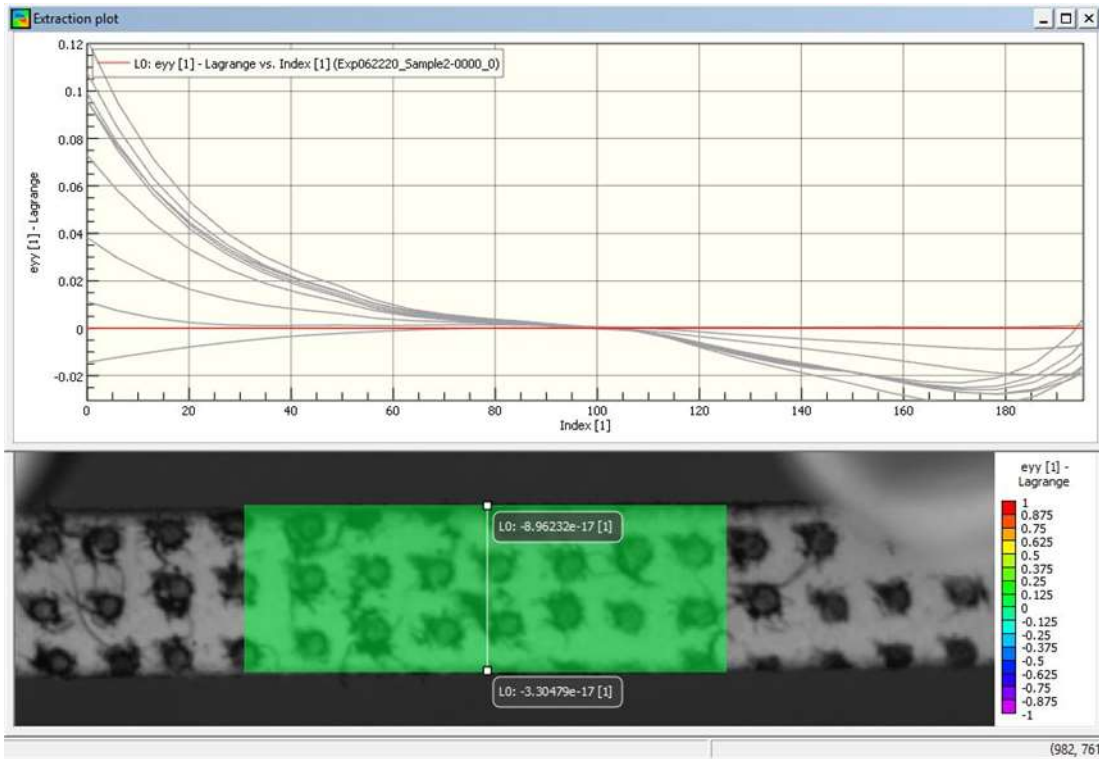

Figure 31. Strain profile in Y-direction for a line L0 in Homogeneous sample -2

5 different points along this line were selected, probed, and their strain profile along X-direction against time has been plotted shown in figure 39.
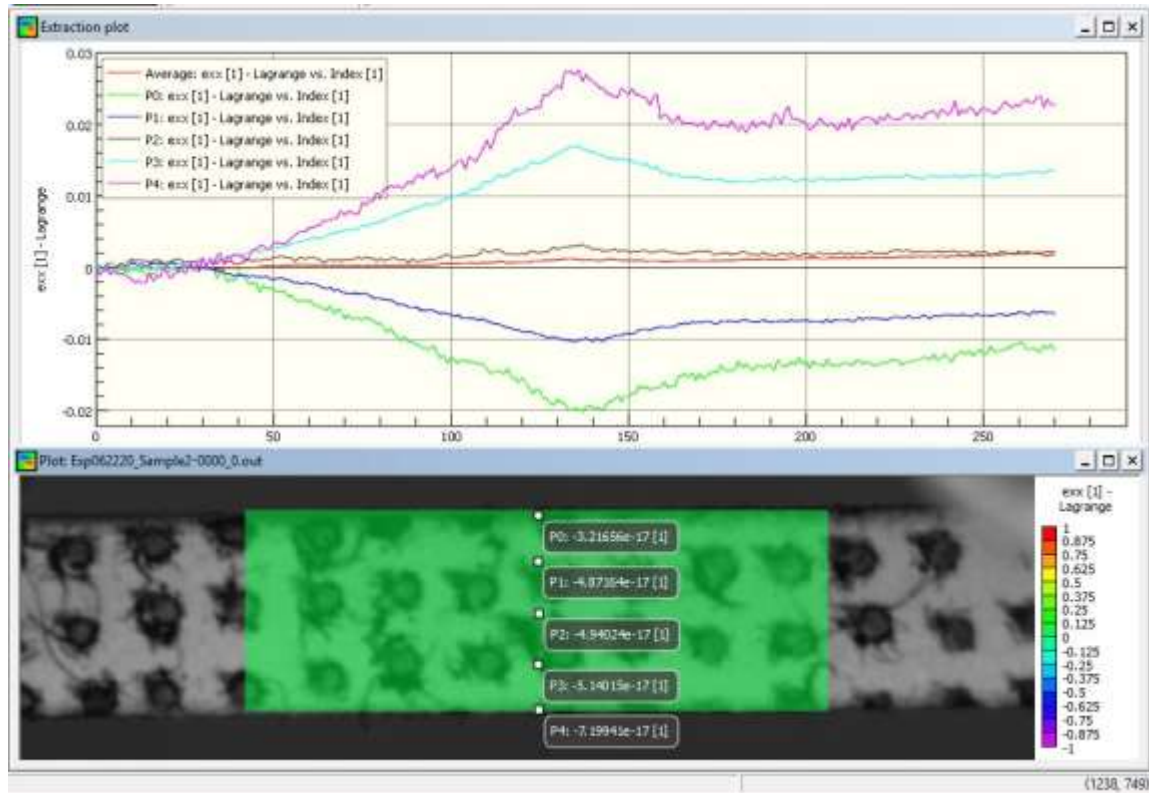
Figure 32. Strain profile in X-direction for 5 points along the line L0 in Homogeneous sample -2

Point P2 is very close to the neutral axis and other points are symmetric/equidistant from point P2 as seen in the figure. The plots validate our expectation, point P0, and P1 are almost equal in magnitude and opposite in direction compared to P4 and P3 respectively. P0, and P1 are in compression P3, and P4 are in tension.

4.1.3.2. Homogeneous sample- 4 (256HV):

This sample's analysis gave us almost similar plots to the previous one, The strain (E_{xx}) is almost 0 at time 0 as seen in the figure (the red line), the neutral axis is at around pixel no. 85 where strain along the x-direction is always zero. The pixel points above the neutral axis undergo gradual compression and below the neutral axis undergo gradual tension when subjected to incremental flexural

loading. There was some data/ correlation loss I got for this sample, but the pattern is pretty similar to the homogeneous sample 2. All these are evident from figure 40.
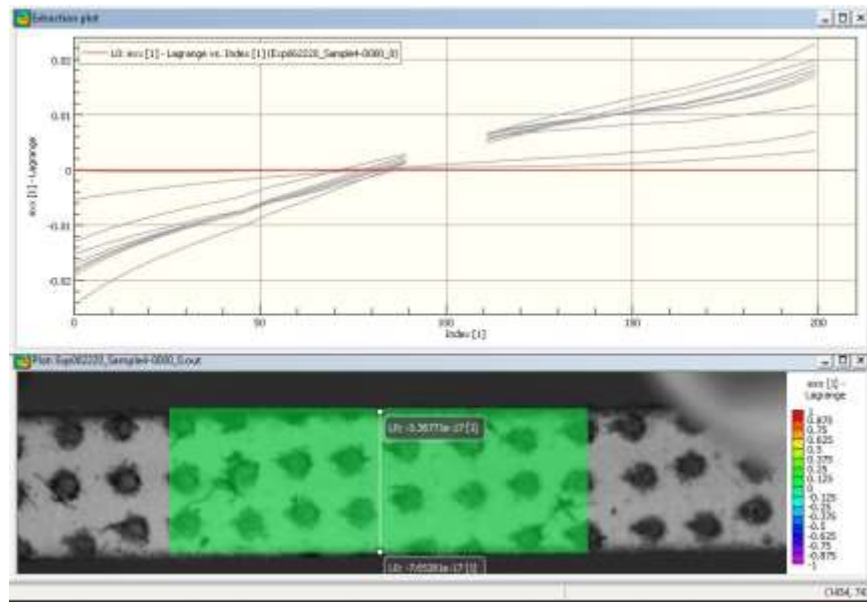

Figure 33. Strain profile in X-direction for a line L0 in Homogeneous sample -4

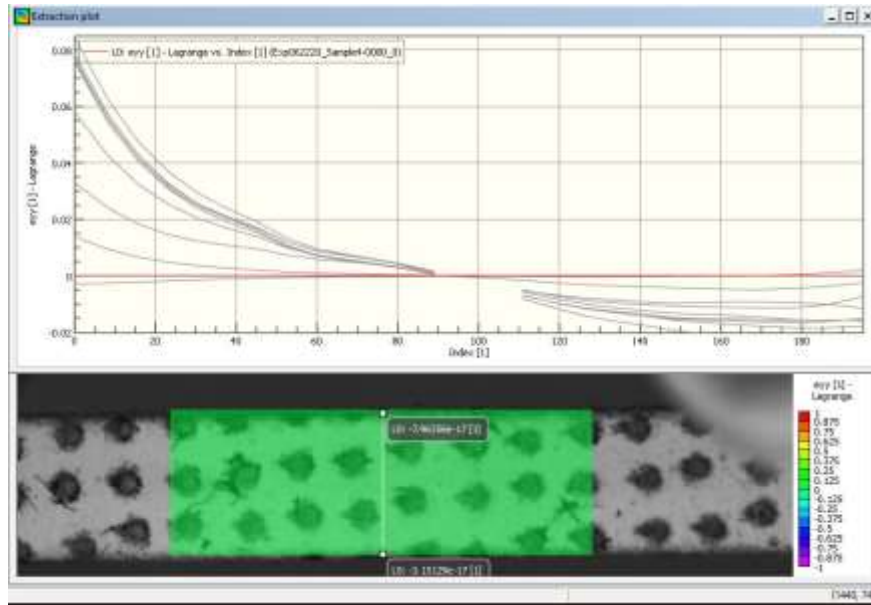The strain profile along the Y- Y-direction (E_{yy}) for line L0 has also been plotted as shown in figure41.

Figure 34. Strain profile in Y-direction for a line L0 in Homogeneous sample -2

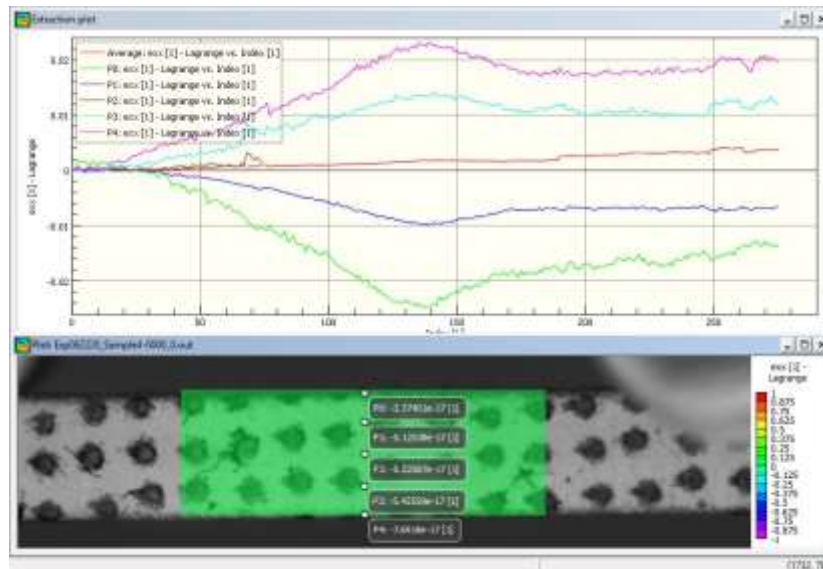E_{xx} has been plotted for five different points probed points along the line L0 is shown in figure

42.

Figure 35. Strain profile in X-direction for 5 points along the line L0 in Homogeneous sample -4

4.1.3.3. Two-zone out high sample:

E_{xx} for line L0is shown in figure 43. The plot is very symmetric to pixel no. 100 which is a point on the neutral axis. It is also symmetric to strain=0 line (red line).
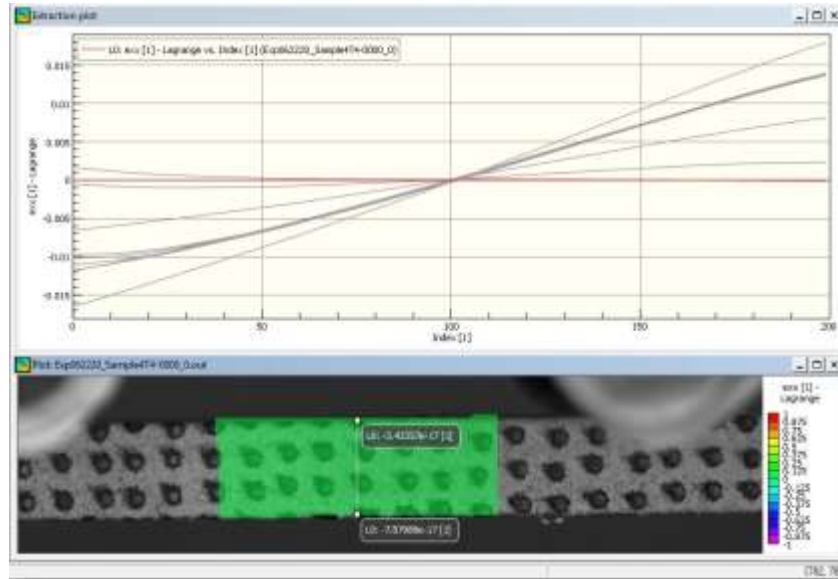

Figure 36. Strain profile in X-direction for a line L0 in 2 Zone out high sample

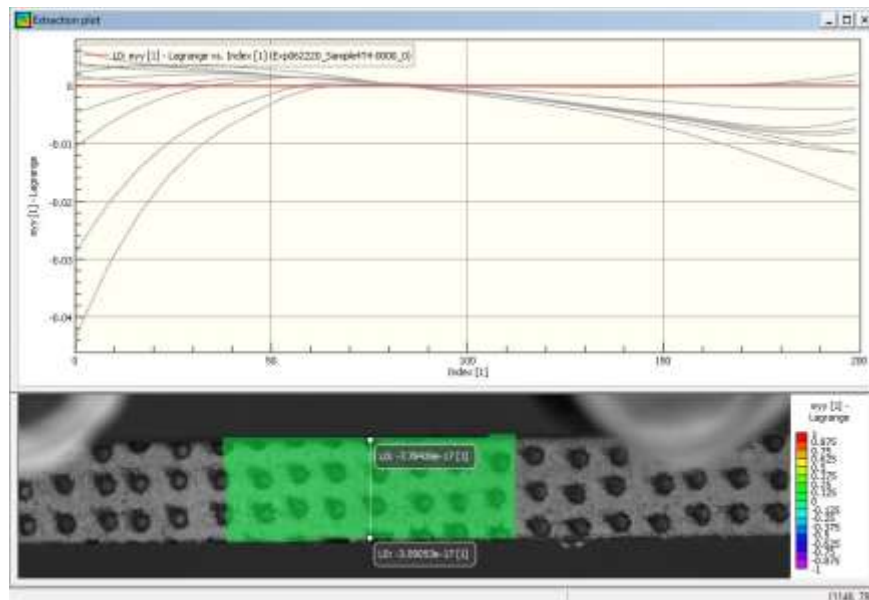E_{yy} for line L0 can be seen in figure 44.

Figure 37. Strain profile in Y-direction for a line L0 in 2 Zone out high sample

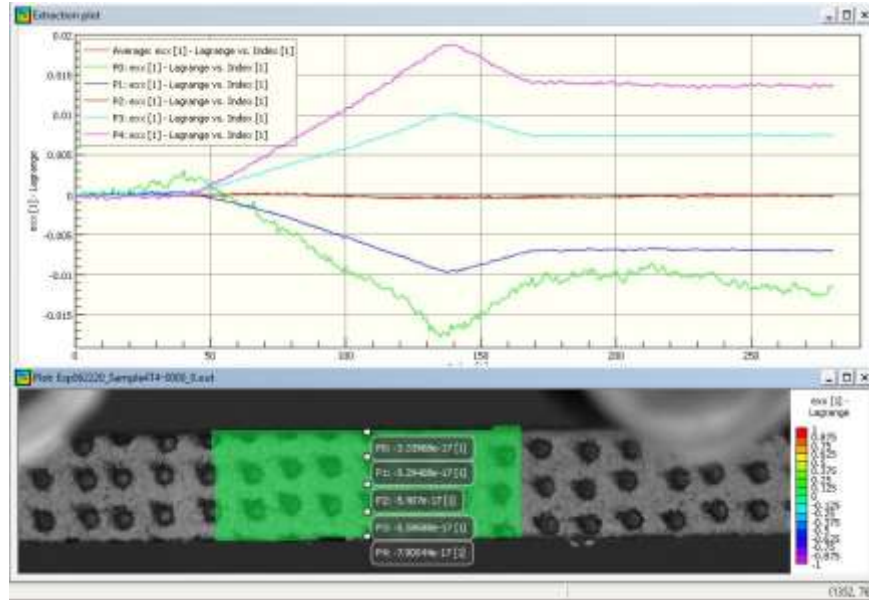E_{xx} for 5 different probed points is shown in figure 45.

Figure 38. Strain profile in X-direction for 5 points along the line L0 in 2 Zone out high sample

4.1.3.4. Two-zone out low sample:

E_{xx} for line L0 (shown in figure 46). Similar in pattern to other samples.
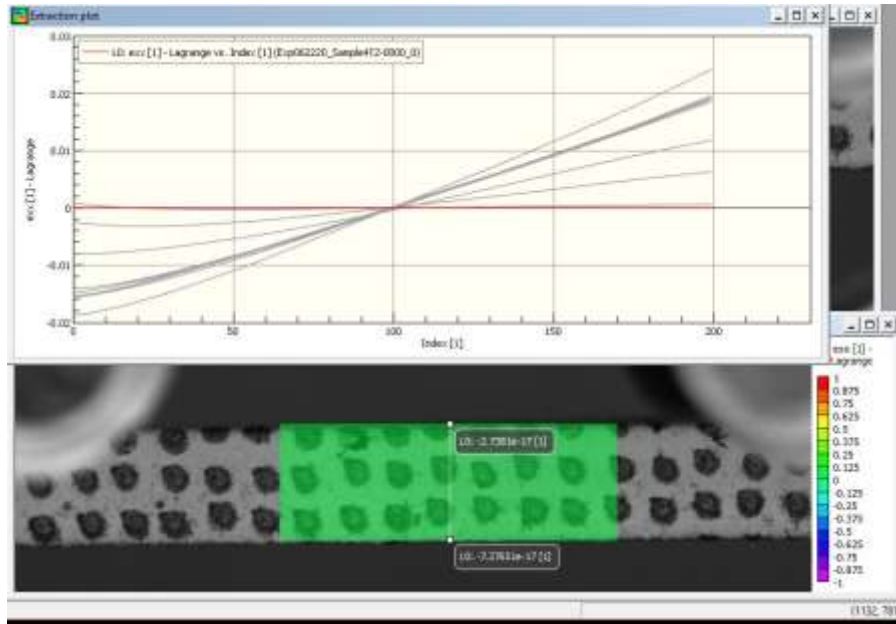
Figure 39. Strain profile in X-direction for a line L0 in 2 Zone out low sample
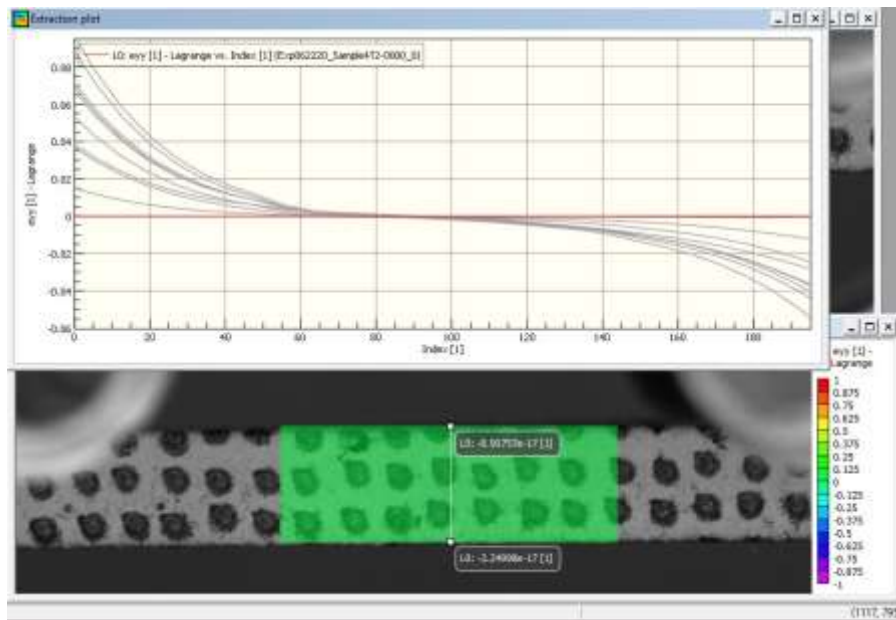
E_{yy} for line L0 (figure 47).

Figure 40. Strain profile in Y-direction for a line L0 in 2 Zone out low sample

E_{xx} for 5 different probe points along line L0 (figure 48).
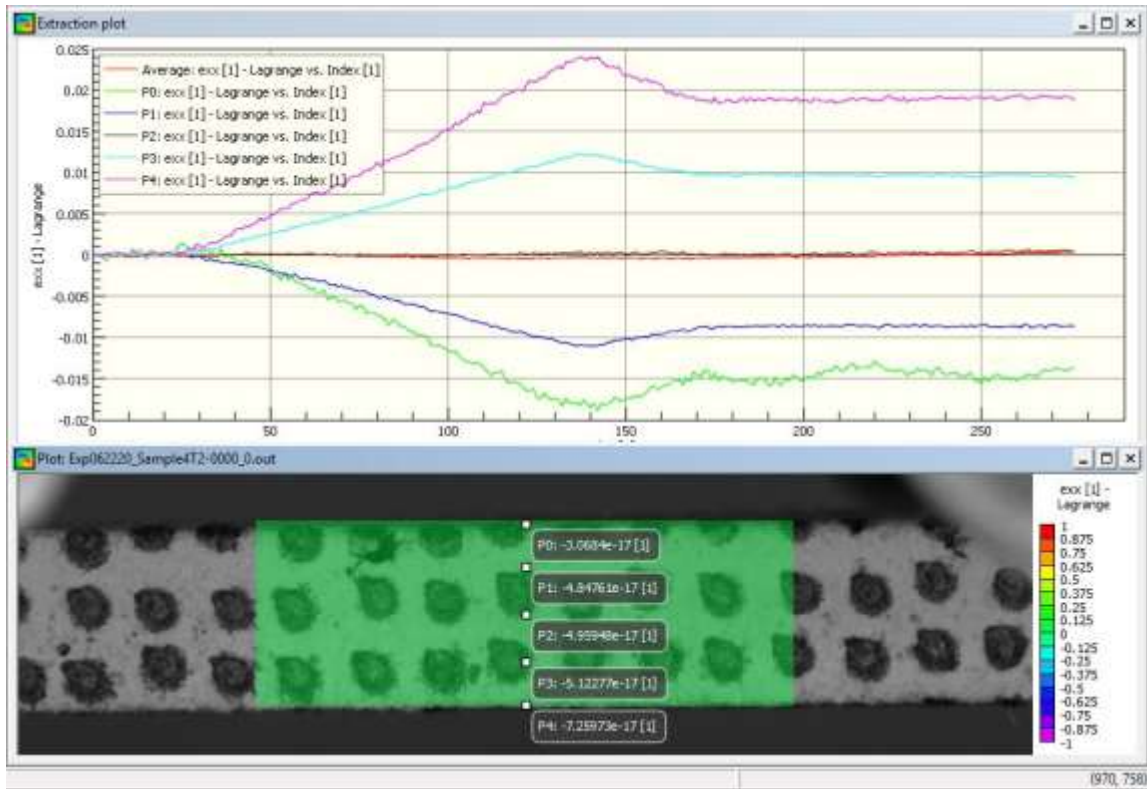
Figure 41. Strain profile in X-direction for 5 points along the line L0 in 2 Zone out low sample

The strain data obtained by carefully counting the pixel for all the samples, those were then compared for all the configurations and have been plotted for all 5 selected points.
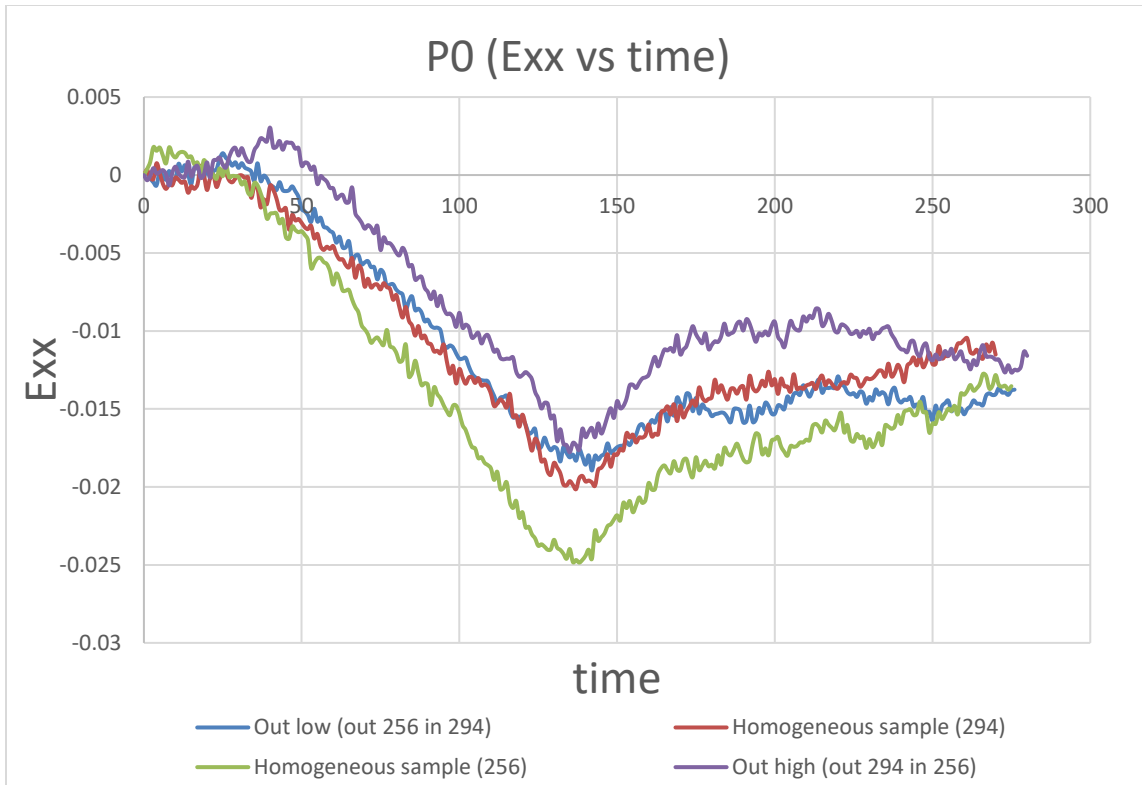
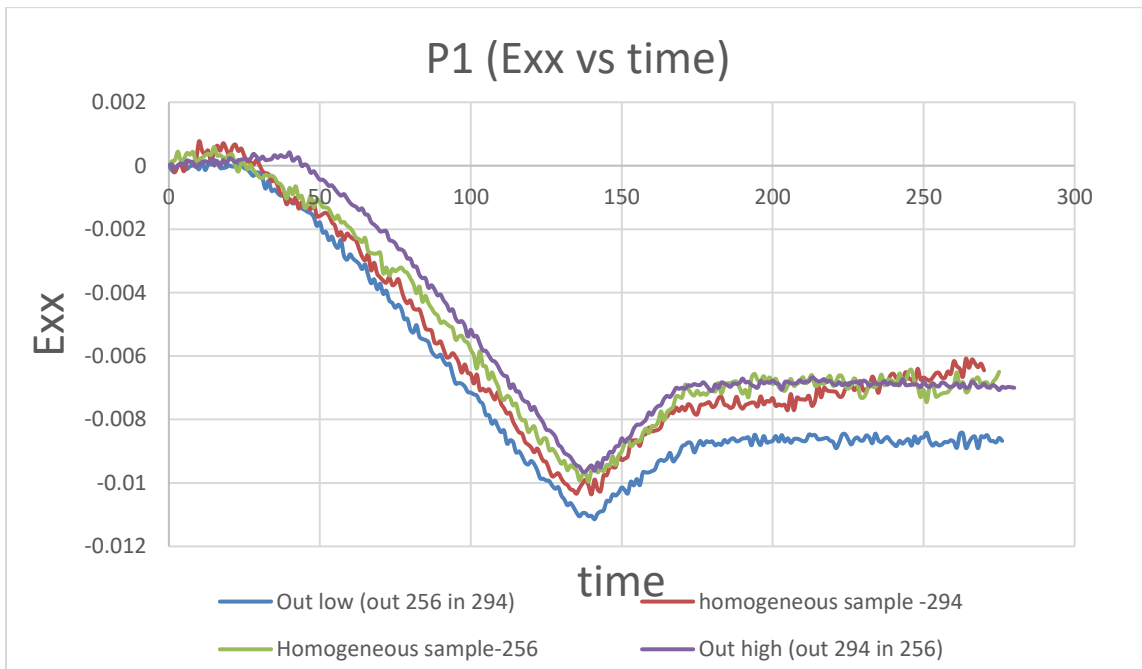**Figure 42. E$_{xx}$ comparison of top point P0 for all 4 configurations**

Figure 43. E$_{xx}$ comparison of top intermediate point P1 for all 4 configurations
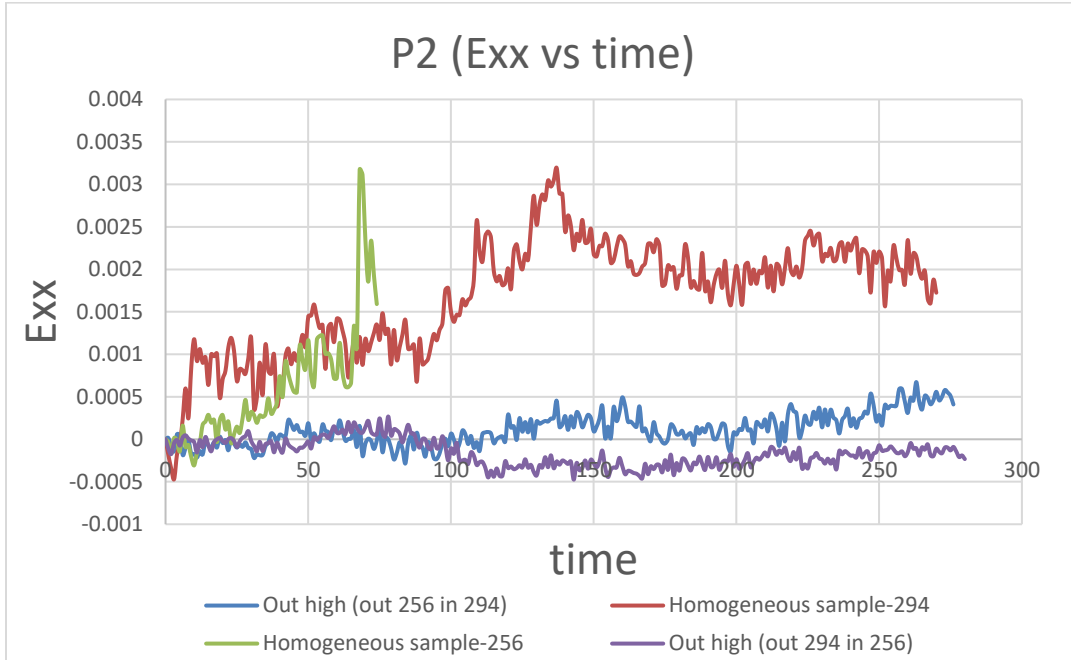
Figure 44. E$_{xx}$ comparison of center point P2 for all 4 configurations
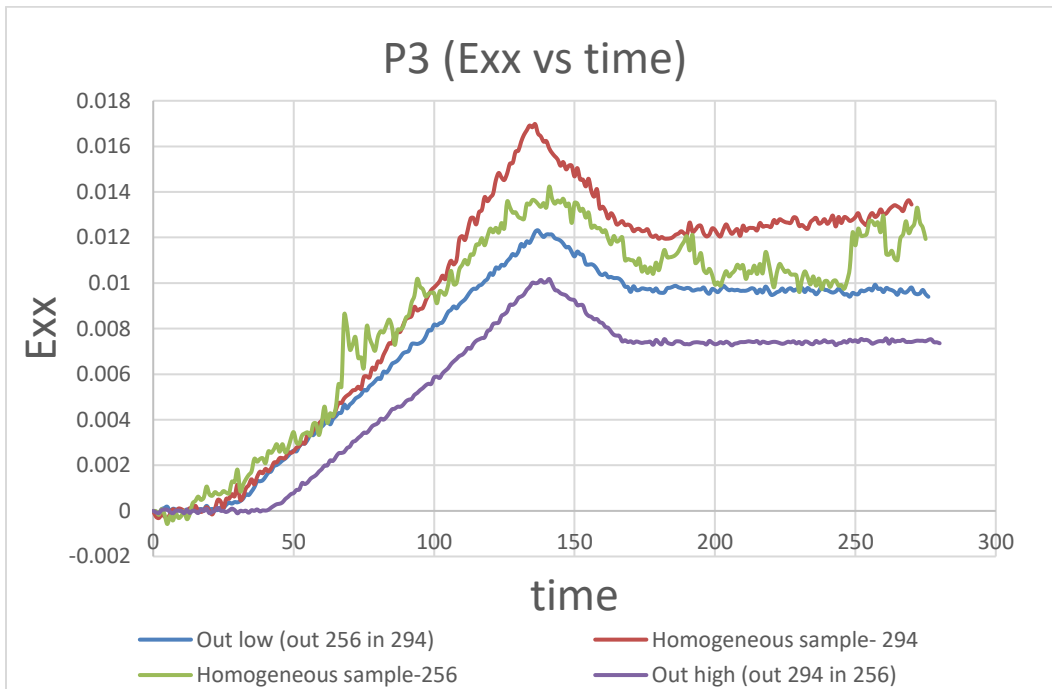
Figure 45. E$_{xx}$ comparison of bottom intermediate point P3 for all 4 configurations
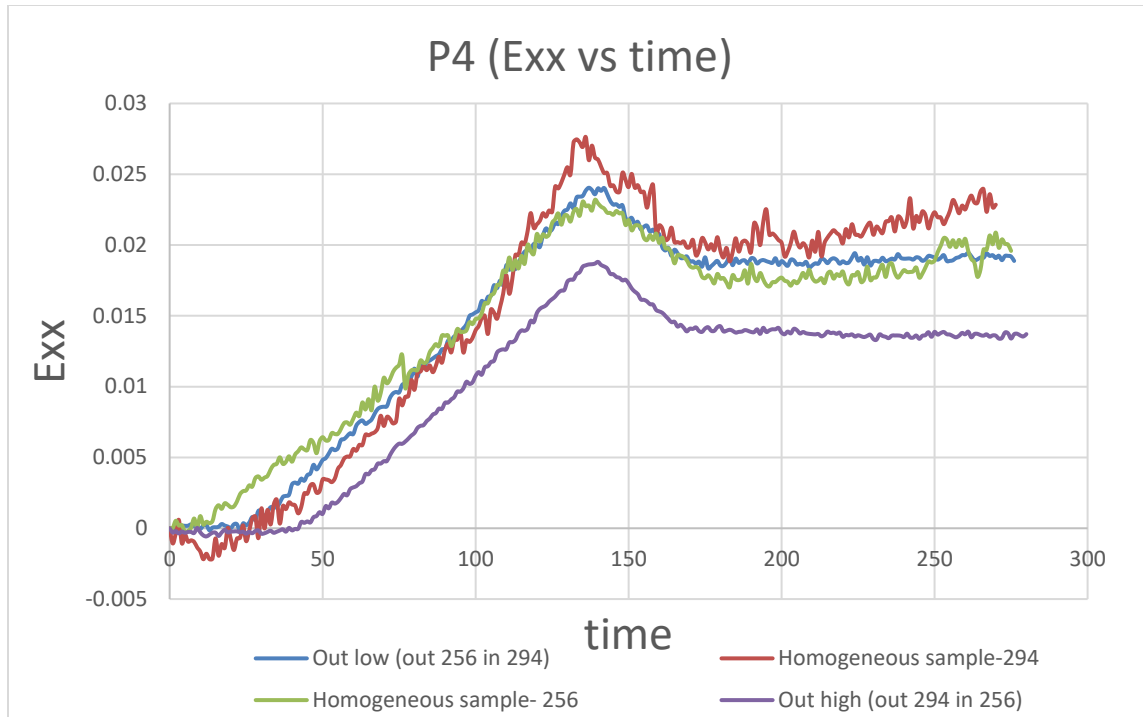
Figure 46. E$_{xx}$ comparison of bottom point P4 for all 4 configurations.

From figure 49 to 53, all 5 probed point's comparison has been plotted. At most points, our expectations are being matched whereas in some cases expectation is not matched. We expect that at the P0 point all the samples should experience compression which is the case. Homogeneous sample-294 should show the lowest strain followed by out high sample, followed by out low samples, followed by homogeneous sample- 256 at all five points which is not the case in these figures. This DIC points plots comparison has to be taken with a grain of salt as the strain experienced by a point is very small so there is a very small margin of comparison. So, the pattern we expect will not necessarily be met.

CONCLUSIONS

In conclusion to this research work, functionally graded samples were manufactured according to the intended hardness grading by systematically altering the location-specific volumetric energy density achieved via the process-parameter change in a selective laser melting process corresponding to the created design of experiments.

Tensile test data showed that most of the samples showed very good repeatability in the elastic as well as plastic regime, but a few samples fractured prematurely during plastic deformation suggesting the existence of manufacturing defects. Most of the samples broke at roughly 25% strain which was expected for SS316L. A few samples showed aberrant behavior in the elastic zone which might be due to some manufacturing alteration of an otherwise 'homogeneous' sample. The slopes for all the samples did not follow the trend we expected according to microhardness.

Our bending test set-2 concludes that the repeatability in load vs deflection for all the configurations was very good. Only 2 samples showed an aberrant slope pattern. This suggests that the manufacturability is very good without any major defects. When these few outliers were excluded, the bulk performance under flexural bending shows that the difference in performance between the configurations is noticeable but not very significant. This is to be expected since the functional gradation is done by changing the power of the laser and exposure time of the energy pulse which doesn't alter the composition, but causes variations in the microstructure and porosity, thus affecting the hardness in an impactful/predictable manner, but the modulus in a not so predictable manner. The slope and elastic modulus under bending mostly correlate to the hardness value but it is not proportional.

In Bending test set 1, the 2 zone out high samples showed very good repeatability whereas the 2 zone out low samples did not show a high degree of repeatability. This is attributed to manufacturing issues. We can also say that the performance of hardness-graded samples did not follow the elastic

modulus expectation. So, hardness and elastic modulus aren't necessarily interchangeable when considering load vs deflection performance.

The DIC analysis for all the samples gave results that matched expectations. For all the samples the spatial and temporal strain profiles across the thickness of the sample in both X and Y directions validated the expectations. The line plots showed that the region over the neutral axis undergoes gradual compression and the region below the neutral axis undergoes gradual tension. The tension and compression in the x-direction are very symmetric to the neural axis as seen in all the images for lines and points probed for various samples. The comparison plots for five similarly placed points on different configurations of samples showed expected behavior in the elastic region. There was some unexpected behavior for some configuration for few probed points but since the strain values are extremely small and locating and probing the same location in every sample has some error associated with it that might lead to such an unexpected pattern.

The bulk performance data showed the slope/elastic modulus of outside high graded samples is greater than outside low graded samples in general. In most cases, the behavior of the homogeneous samples was intermediate, but there exist some instances where homogeneous samples did not behave intermediately. In general, elastic modulus and slopes behavior pattern mostly correlate with the hardness value but the relationship is not directly proportional. Further, the hardness turned out to be a more reliable control parameter for functional gradation than the elastic modulus. The functional gradation had small but noticeable performance implications compared to non-graded parts. These hardness graded materials will have very applicability in situations where depth-dependent hardness will be required, *e.g.*, wear resistance, inhibition of crack initiation, etc. Altogether, functionally graded materials discussed in this research work or similar materials will have very good application in

structural engineering, automotive, many other fields where performance gain/control under bending is intended.

5.1. Future Work

Some of the future works that can be extended to this research work are evaluating the performance of such hardness and stiffness graded structures under cyclic fatigue loading and implementing finite element analysis (FEA) to validate and extend the results of tensile and bending tests as well as on fatigue tests. Vibration and buckling can also be investigated for such functionally graded samples. Apart from that more combinations of parameters should be tried to achieve more disparate functional gradation with respect to hardness as well as elasticity.

REFERENCES

1. Chauhan, P.K. and S. Khan, *Microstructural examination of aluminium-copper functionally graded material developed by powder metallurgy route.* Materials Today: Proceedings, 2020. **25**: p. 833-837.

2. Loh, G.H., et al., *An overview of functionally graded additive manufacturing.* Additive Manufacturing, 2018. **23**: p. 34-44.

3. Bobbio, L.D., et al., *Additive manufacturing of a functionally graded material from Ti-6Al-4V to Invar: Experimental characterization and thermodynamic calculations.* Acta Materialia, 2017. **127**: p. 133-142.

4. Leu, M.C., et al., *Freeze-form extrusion fabrication of functionally graded materials.* CIRP annals, 2012. **61**(1): p. 223-226.

5. Muller, P., P. Mognol, and J.-Y. Hascoet, *Modeling and control of a direct laser powder deposition process for Functionally Graded Materials (FGM) parts manufacturing.* journal of materials processing technology, 2013. **213**(5): p. 685-692.

6. Yan, W., et al., *Multi-scale modeling of electron beam melting of functionally graded materials.* Acta Materialia, 2016. **115**: p. 403-412.

7. Yin, S., et al., *Hybrid additive manufacturing of Al-Ti6Al4V functionally graded materials with selective laser melting and cold spraying.* Journal of Materials Processing Technology, 2018. **255**: p. 650-655.

8. Mahamood, R. and E.T. Akinlabi, *Laser metal deposition of functionally graded Ti6Al4V/TiC.* Materials & Design, 2015. **84**: p. 402-410.

9. Yan, L., Y. Chen, and F. Liou, *Additive manufacturing of functionally graded metallic materials using laser metal deposition.* Additive Manufacturing, 2020. **31**: p. 100901.

10. Wu, D., et al., *Laser rapid manufacturing of stainless steel 316L/Inconel718 functionally graded materials: microstructure evolution and mechanical properties.* International Journal of Optics, 2010. **2010**.

11. Carroll, B.E., et al., *Functionally graded material of 304L stainless steel and inconel 625 fabricated by directed energy deposition: Characterization and thermodynamic modeling.* Acta Materialia, 2016. **108**: p. 46-54.

12. Nam, S., et al., *Effect of process parameters on deposition properties of functionally graded STS 316/Fe manufactured by laser direct metal deposition.* Metals, 2018. **8**(8): p. 607.

13. Zhong, Y., et al., *Additive manufacturing of 316L stainless steel by electron beam melting for nuclear fusion applications.* Journal of nuclear materials, 2017. **486**: p. 234-245.

14. Niendorf, T., et al., *Functionally graded alloys obtained by additive manufacturing.* Advanced engineering materials, 2014. **16**(7): p. 857-861.

15. Zhang, K., et al., *Characterization of stainless steel parts by laser metal deposition shaping.* Materials & Design, 2014. **55**: p. 104-119.

16. Sola, A., D. Bellucci, and V. Cannillo, *Functionally graded materials for orthopedic applications–an update on design and manufacturing.* Biotechnology advances, 2016. **34**(5): p. 504-531.

17.   Popoola, P., et al., *Laser Engineering Net Shaping Method in the Area of Development of Functionally Graded Materials (FGMs) for Aero Engine Applications-A Review*. Fiber Laser, 2016: p. 383-399.

18.   Khan, S., *Analysis of tribological applications of functionally graded materials in mobility engineering*. Int. J. Sci. Eng. Res, 2015. **6**(3): p. 1150-1160.

19.   Kanu, N.J., et al., *Fracture problems, vibration, buckling, and bending analyses of functionally graded materials: A state-of-the-art review including smart FGMS*. Particulate Science and Technology, 2019. **37**(5): p. 583-608.

20.   Gupta, N., S.K. Gupta, and B.J. Mueller, *Analysis of a functionally graded particulate composite under flexural loading conditions*. Materials Science and Engineering: A, 2008. **485**(1-2): p. 439-447.

21.   Ke, L.-L., et al., *Bending, buckling and vibration of size-dependent functionally graded annular microplates*. Composite structures, 2012. **94**(11): p. 3250-3257.

22.   Jajarmi, E. and S.A. Sajjadi, *Fractography of 3YPSZ/316L functionally graded composite subjected to indentation and flexural bending tests*. Ceramics International, 2017. **43**(14): p. 11281-11288.

23.   ASTM International. *Standard Test Method for Flexural Strength of Advanced Ceramics at Ambient Temperature*. 2018; Available from: http://www.astm.org/cgi-bin/resolver.cgi?C1161-18.